

Review

# A Review of the Laser Cladding of Metal-Based Alloys, Ceramic-Reinforced Composites, Amorphous Alloys, and High-Entropy Alloys on Aluminum Alloys

Pengfei Zhao <sup>1,2</sup>, Zimu Shi <sup>3</sup>, Xingfu Wang <sup>3</sup>, Yanzhou Li <sup>4</sup> , Zhanyi Cao <sup>1</sup>, Modi Zhao <sup>3,\*</sup> and Juhua Liang <sup>3,\*</sup>

<sup>1</sup> Key Laboratory of Automobile Materials, Ministry of Education, College of Materials Science and Engineering, Jilin University, Changchun 130022, China; zhaopf16@mails.jlu.edu.cn (P.Z.); caozy@jlu.edu.cn (Z.C.)

<sup>2</sup> College of Information Engineering, Jilin Vocational College of Industry and Technology, Jilin 132012, China

<sup>3</sup> Key Laboratory of Materials Physics, Institute of Solid State Physics, Chinese Academy of Sciences, Hefei 230031, China; shizimu@issp.ac.cn (Z.S.); wangxingfu@issp.ac.cn (X.W.)

<sup>4</sup> School of Mechanical and Vehicle Engineering, West Anhui University, Luan 237010, China; liyanzhou9336@163.com

\* Correspondence: mdzhao@issp.ac.cn (M.Z.); liangjuhua0721@126.com (J.L.); Tel.: +86-15044211299 (J.L.)

**Abstract:** As one of the lightest structural metals, the application breadth of aluminum alloys is, to some extent, constrained by their relatively low wear resistance and hardness. However, laser cladding technology, with its low dilution rate, compact structure, excellent coating-to-substrate bonding, and environmental advantages, can significantly enhance the surface hardness and wear resistance of aluminum alloys, thus proving to be an effective surface modification strategy. This review focuses on the topic of surface laser cladding materials for aluminum alloys, detailing the application background, process, microstructure, hardness, wear resistance, and corrosion resistance of six types of coatings, namely Al-based, Ni-based, Fe-based, ceramic-based, amorphous glass, and high-entropy alloys. Each coating type's characteristics are summarized, providing theoretical references for designing and selecting laser cladding coatings for aluminum alloy surfaces. Furthermore, a prediction and outlook for the future development of laser cladding on the surface of aluminum alloys is also presented.

**Keywords:** aluminum alloy; laser cladding; material system; research status



**Citation:** Zhao, P.; Shi, Z.; Wang, X.; Li, Y.; Cao, Z.; Zhao, M.; Liang, J. A Review of the Laser Cladding of Metal-Based Alloys, Ceramic-Reinforced Composites, Amorphous Alloys, and High-Entropy Alloys on Aluminum Alloys. *Lubricants* **2023**, *11*, 482. <https://doi.org/10.3390/lubricants11110482>

Received: 4 October 2023

Revised: 28 October 2023

Accepted: 2 November 2023

Published: 8 November 2023



**Copyright:** © 2023 by the authors. Licensee MDPI, Basel, Switzerland. This article is an open access article distributed under the terms and conditions of the Creative Commons Attribution (CC BY) license (<https://creativecommons.org/licenses/by/4.0/>).

## 1. Introduction

Aluminum and its alloys are regarded as one of the most pivotal metal materials of the 21st century [1,2]. Its content in the earth's crust is as high as 7.73%, ranking third, following only oxygen and silicon, which makes it the most abundant of the metallic elements. The tensile strength of pure aluminum (with an aluminum content not less than 99.60%) is 70–130 MPa, its elongation rate is 6–43%, and its hardness is 35 HB [2–9]. An aluminum alloy is made by adding some other elements to pure aluminum. Thus, its performance outperforms pure aluminum. Aluminum alloys possess high specific stiffness, high specific strength, excellent corrosion resistance, and easy processability [10–12]. It is not only widely used in aerospace, rail transit, shipbuilding, automotive, and military fields, but its development trend is towards larger sizes, integration, complex shapes, and high precision, making it the first choice for lightweight design [12–22].

However, the surface of aluminum alloys is soft, lacking high wear and heat resistance [23–25]. This restricts its application in mechanical parts requiring high surface hardness, wear resistance, and heat resistance [26–28]. Meanwhile, with the rapid development of the equipment manufacturing industry, many critical components of mechanical equipment have failed and been scrapped in harsh and complex environments, causing tremendous economic losses and a high equipment failure rate. There is an urgent need to

explore efficient, green, emerging manufacturing technologies to enhance the lifespan of crucial new parts and remanufacture and repair outdated equipment.

Surface modification technology can be used to improve the surface performance of these parts. Currently, relatively mature surface modification technologies include thermal spraying, physical vapor deposition, electroplating, and laser cladding [29–32]. Among these, the most developed technologies are thermal spraying, physical vapor deposition, and electroplating. Even though they can effectively improve the surface performance of aluminum alloys, they all have specific issues. For instance, thermal spraying can form a thick coating, but inclusions and pores may appear, leading to poor bonding. The coating produced via physical vapor deposition is thin, and the high-temperature working environment may cause organizational changes at the bottom of the coating, resulting in the peeling of the coating [28]. The coating produced via electroplating is not dense enough, and the electroplating solution causes significant environmental pollution. Laser cladding technology has emerged with the development of laser and surface modification technologies [33–38]. By utilizing a laser beam to melt the cladding material and the surface of the base body and allowing it to solidify to form a cladding layer that metallurgically bonds with the base body, it can be used for the surface strengthening of new parts and the remanufacturing and repair of failed parts [39–42].

Laser surface modification technology occupies an advanced position in surface engineering. Its research began in the 1960s, but it was not until the early 1970s that it was practically applied [37,38,43]. The technique is widely acknowledged for its efficiency, pollution-free nature, and low material consumption. At its core, it uses lasers as a heat source to treat the surface of the metallic materials, optimizing their microstructure, phase structure, and chemical composition to enhance surface properties. Unlike traditional whole-body heat treatments, the laser only affects the surface, preserving the overall material properties. Its key features include a high heating speed, high power density, minimal heat-affected zones, adaptability to complex parts, energy reduction, cost reduction, and suitability for automation. The main processes include laser phase transformation hardening, melting hardening, laser shock hardening, laser alloying, and laser cladding.

Laser phase transformation hardening involves rapidly scanning the workpiece with a high-energy laser beam, bringing the surface to a phase change point below the melting point at a heating rate  $10^4\sim 10^6$  °C/s [44,45]. The cooler workpiece substrate then undergoes rapid self-quenching at a cooling rate of  $10^4\sim 10^8$  °C/s, creating the surface phase transformation hardening. Laser melting hardening uses a laser beam of extremely high power density to instantly heat a localized metal surface region above its melting point [46–48]. Then, through the cooling effect of the cold metal substrate, the thin melted metal surface rapidly solidifies, resulting in a modified surface layer that may or may not have the same composition as the substrate but possesses different properties. This technique applies to both ferrous and non-ferrous metals and not only corrects surface defects like pores, cracks, and impurities but also enhances surface performance.

Furthermore, it can be employed for remelting plasma-sprayed coatings that are wear-resistant, heat-resistant, and corrosion-resistant, and for remelting laser-clad coatings, making it highly versatile. Laser shock hardening irradiates the metal workpiece surface with a short-pulse laser of ultra-high power density, causing the surface material to rapidly vaporize and generate shockwaves with pressures up to  $10^4$  Pa [49–51]. This leads to a significant toughening deformation on the metal surface, resulting in hardening. The microscopic structure in the laser shock zone showcases a complex network of tangled dislocations, akin to the substructures seen in materials post-explosion or rapid planar shock, significantly enhancing the material's surface strength, yield strength, and fatigue life.

Laser alloying melts the substrate metal surface using a high-energy laser while introducing alloying elements [52,53]. This forms a concentrated, uniformly mixed alloy layer on the substrate surface, giving it resistance to wear, corrosion, and high-temperature oxidation. Due to the swift nature of laser alloying, solute elements primarily achieve uniformity through liquid-state convection. This means that the composition of the laser alloy

can greatly differ from conventional alloy compositions. Moreover, the process can replace expensive whole alloy substrates with cheaper base materials, reducing manufacturing costs and substantially improving production efficiency. Methods like preset material, synchronous powder feeding, and laser gas alloying are employed during laser alloying.

Laser cladding, a branch of laser surface modification, was first researched in the 1970s, emerging with the development of high-power lasers. Here, cladding material is added to the workpiece surface. When exposed to a high-energy laser, both the cladding material and a thin layer of the substrate metal melt quickly, then rapidly solidify into a clad layer, resulting in a modified or coated layer with the desired properties. The power density distribution for laser cladding ranges between  $10^4$  and  $10^5$  W/cm<sup>2</sup>, positioning it between laser hardening and laser alloying in terms of application. Laser cladding, compared with traditional surface modification technologies, has many advantages: it applies to a wide range of material systems; enables rapid heating and swift cooling, leading to the refinement of the cladding layer composition; has a low dilution rate, and bonds well with the substrate; has a minimal heat-affected zone on the base material; offers high energy utilization rate; and is an environmentally friendly process [54,55]. Therefore, the laser cladding of aluminum alloys has broad development prospects. However, it is not without its challenges. The equipment and operational costs associated with laser cladding can be high. The technique also demands precise control over laser parameters; mismanagement can induce defects like cracking, porosity, or unwanted phase formations.

Additionally, there are potential risks of substrate damage from excessive laser energy, and the process requires skilled operators for optimal outcomes. Laser cladding has found extensive applications in sectors like oil and gas, aerospace, and automotives, enhancing wear and corrosion resistance despite its limitations. It is also invaluable for restoring or repairing complex or costly components, demonstrating its significance in contemporary material engineering.

Laser cladding technology integrates laser technology, computer-assisted manufacturing, and automated control technology. It is worth noting that aluminum alloys have a strong reflective effect on laser beams, with their reflectivity mainly inversely proportional to the wavelength of the laser [38,56]. Aluminum's interaction with electromagnetic radiation, particularly in the visible and infrared regions, is dictated by its dielectric function and interband transitions. Aluminum's high reflectivity arises from its conduction-electron solid response, governed by its free electrons. Spectrally, aluminum exhibits increased reflectivity for longer wavelengths, which is clearly evidenced by its response to different lasers. For instance, for a CO<sub>2</sub> laser with a wavelength of 10.6 μm, the laser reflectivity is as high as 90%. For a Nd: YAG laser with a wavelength of 1.06 μm, the absorption rate is seven times that of a CO<sub>2</sub> laser. Radiation photo-absorbent materials can enhance absorptivity to address this challenge, especially in more extended wavelength lasers. The application of laser cladding on aluminum alloys is closely tied to developing a high-quality, high-power laser.

Laser cladding technology uses the laser beam's energy to simultaneously melt the coating powder and the surface of the substrate, forming a well-bonded coating when the laser beam moves away and the molten pool solidifies quickly. Therefore, laser cladding technology has the advantages of high processing efficiency, high-quality coating preparation, and environmental friendliness.

Two types can be distinguished depending on the method of inputting cladding materials: the pre-placed powder method and the synchronous powder feeding method, as depicted in Figure 1 [38]. The pre-placed powder method is simple to operate. However, due to its lower-quality cladding layer, it is not suitable for industrial production. The synchronous powder feeding method, including synchronous side feeding and coaxial feeding, provides excellent-quality cladding layers and is conducive to automated control.

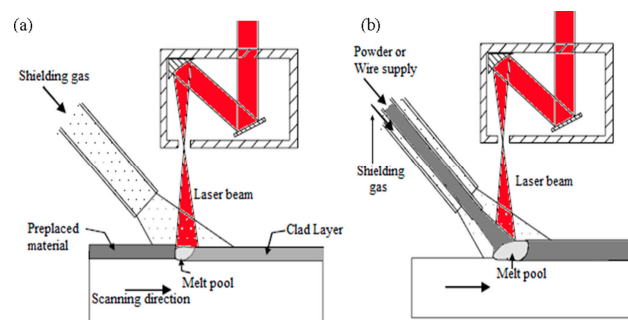


**Figure 1.** Schematic diagram of laser cladding ((a) is the pre-placed powder method; (b) is the synchronous powder feeding method) [38].

As shown in Figure 2, the geometric shape of the laser cladding layer typically includes the height ( $H$ ), width ( $D$ ), depth ( $h$ ), wetting angle ( $\theta$ ), and dilution rate ( $y$ ) of the cladding layer. The dilution rate  $y$  can be mathematically represented by the formula  $y = h / (h + H)$ . Selecting appropriate cladding materials and sensible cladding process parameters is vital to acquiring a well-formed, high-performance, high-quality cladding layer. The choice of cladding material will determine the performance of the cladding layer. In contrast, the cladding process parameters will directly influence the layer's geometric shape, structure, and performance. Standard parameters for the laser cladding process include laser power, scanning speed, spot diameter, overlap rate, degree of dilution, and the quantity of powder supplied, which is an influential factor in determining the thickness of the coating.

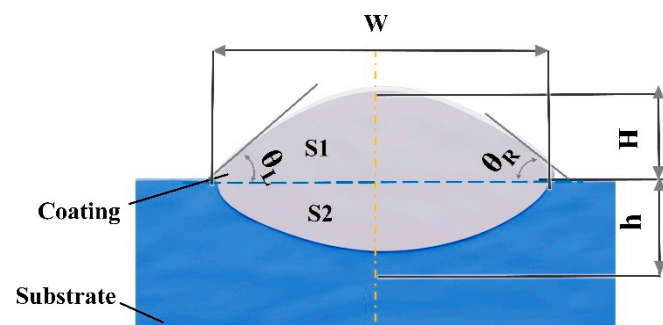


**Figure 2.** Cross-section diagram of the cladding layer.

Currently, the primary material systems for the laser cladding of aluminum alloys include metal-based alloys, ceramic-reinforced composites, and emerging materials such as amorphous and high-entropy alloys. These cladding materials typically come in powder, wire, or sheet form, of which the powder form is the most widely used in industrial applications. This article mainly compared aluminum alloy laser cladding based on the cladding material system. It details the process of using powder cladding materials under different experimental conditions and their forming and organizational performance. It identifies current issues with applying other component powders in the laser cladding of aluminum alloy surfaces. Finally, we summarize and forecast the future development of the laser cladding of aluminum alloys.

## 2. Metal Based Alloys

In the field of laser cladding technology, research on metal-based coatings for aluminum alloy surfaces predominantly focuses on three primary categories: Al-based, Fe-based, and Ni-based coatings.

### 2.1. Al-Based Alloys

Due to its low heat input and high automation, laser cladding technology has been widely applied in metal repair, especially in restoring Al-based alloys. Many scholars have reported on this.

Meinert et al. [57] first laser-clad the 4000 series aluminum alloy onto the surface of 6061 and 7075 aluminum alloys. They found that the tensile strength of the repaired specimens was 61% and 64% of the original 6061-T6 and 7075-T651 samples, respectively. Cottam et al. [58] studied the laser cladding of a 7075 aluminum alloy powder on the surface of a 7075 aluminum alloy. The hardness of the cladding layer they prepared was about 80% of the matrix. Heat treatment can bolster the hardness of the coating, yet it concurrently amplifies the residual stress within the coating. Figure 3 is pivotal in illustrating the sample's residual stress distribution, a key factor influencing the material's performance and durability. To be precise, Figure 3a–c map out the stress distribution in the substrate, the as-clad coating, and the heat-treated coating, respectively. A nuanced evaluation reveals that the substrate exhibits the most average residual stress. Importantly, this figure underscores the transformative effect of the heat treatment: the residual stress in the coating treatment is approximately double that of the as-clad coating. Such insights emphasize the critical nature of understanding and controlling residual stresses in various processing conditions.

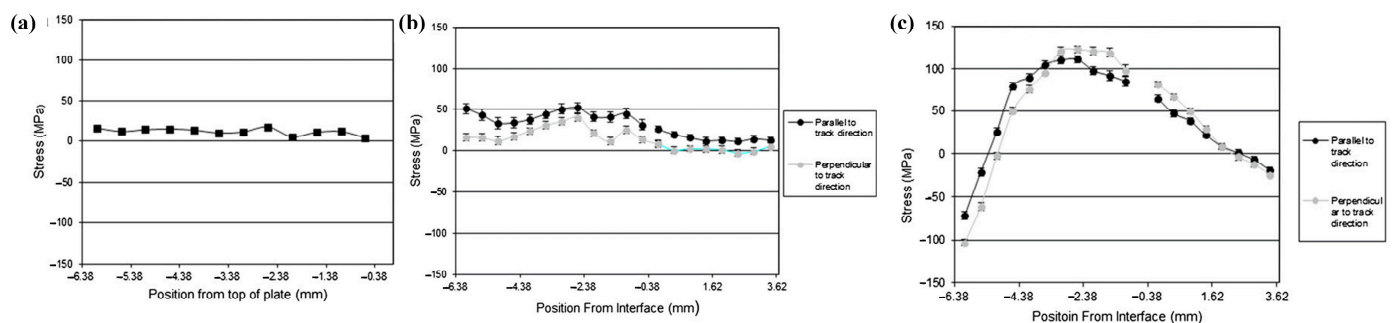


**Figure 3.** The residual stress of (a) substrate; (b) as-clad sample; (c) heat-treated samples [58].

Corbin et al. [59] conducted a study where they applied laser cladding to deposit 6061-T6 aluminum alloy powder onto the surface of a 6061 aluminum alloy substrate. Figure 4 represents the cladding's cross-sectional images, with Figure 4a demonstrating the cladding on the narrow substrate and Figure 4b displaying the coverage on the wide substrate. It can be found that there are no apparent defects, such as pores and cracks, in the single coating. They observed the presence of coarse and sparse  $\beta'$  precipitates in the cladding layer, resulting in a lower hardness than the substrate. In the heat-affected zone, fine and abundant  $\beta''$  precipitates were maintained, which resulted in hardness levels similar to the substrate in that region. These studies indicate that in aluminum alloy repair technology, the performance of the cladding layer is generally lower than that of the aluminum matrix, and issues such as abrupt changes in hydrogen solubility, alloy element ablation, poor powder fluidity, and ease of oxidation exist. Therefore, some researchers have conducted in-depth studies on aluminum alloy repair technology for aspects such as powder feeding devices, process optimization, and post-welding treatment to improve the quality of the cladding layer.

Yang et al. [60] used a high-power diode laser to repair ZL205A aluminum alloy casting defects, which then went through a solution treatment in water at 535 °C for 11 h, followed by artificial aging at 175 °C for 5 h; the hardness of the coating was increased to 134 HV. In contrast to Corbin's research, significant pores were found in the cladding layer. Figure 5 depicts the cross-sectional morphology of the coating, with Figure 5a showing the macroscopic interface and Figure 5b highlighting the pore features.

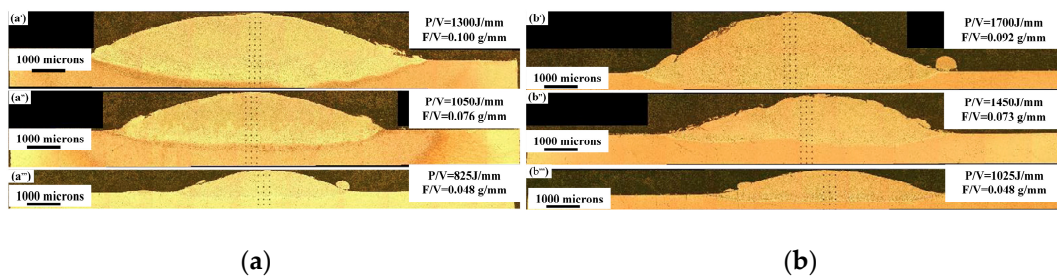


**Figure 4.** The cross-sectional images of the claddings produced on (a) narrow substrate and (b) wide substrate [59].

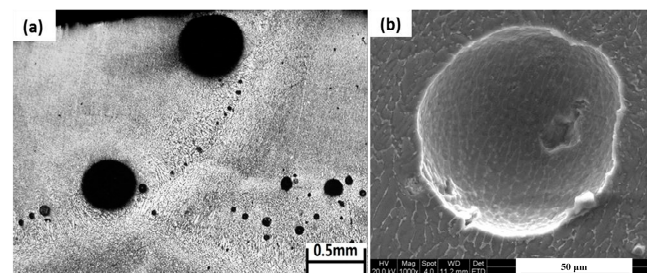


**Figure 5.** Coating morphology with (a) illustrating the cross-sectional view and (b) showing the pore SEM imaging [60].

Regarding process optimization, Song et al. [61] have conducted research to enhance the damage tolerance of aircraft skin. Their approach centers on exploring the benefits of laser cladding aluminum alloy structures for improved crack resistance. They developed a three-dimensional finite element simulation model, incorporating a double ellipsoid heat source and the sequentially coupled thermal–mechanical analysis method. Figure 6 depicts the residual stress distribution in cladded samples under varying laser powers. It was discovered that with increased laser power, the residual compressive stress in the models was enhanced due to an increase in heat energy input, which broadened the thermal influence range and intensified the temperature gradient in the heat-affected zone. This amplified the stress response, particularly in areas where the coating meets the substrate. Their findings suggest that the laser cladding samples reach peak crack resistance at a laser power of 1400 W and a laser scanning velocity of 10 mm/s. Remarkably, they discovered that a sample with a cladding coating length of 50 mm exhibited a fatigue life that was 2.93 times longer than an untreated sample. Moreover, their research points to the superior crack resistance performance of a linear pattern compared to other patterns, with the cladding angle of the linear design at “0” resulting in the highest performance. This research underscores the enhanced fatigue life of samples treated with laser cladding, a benefit attributed to the induced residual compressive stress from the laser cladding process.

Additionally, they found that modifying the laser parameters, such as increasing the laser power or reducing the laser scanning velocity, could further extend the fatigue life of laser-treated samples. The study concludes that various factors, including laser parameters, laser cladding patterns, and angles, can influence the fatigue life of the samples. Some researchers also prepared aluminum-based coatings on the surface of aluminum alloys to improve their surface performance.

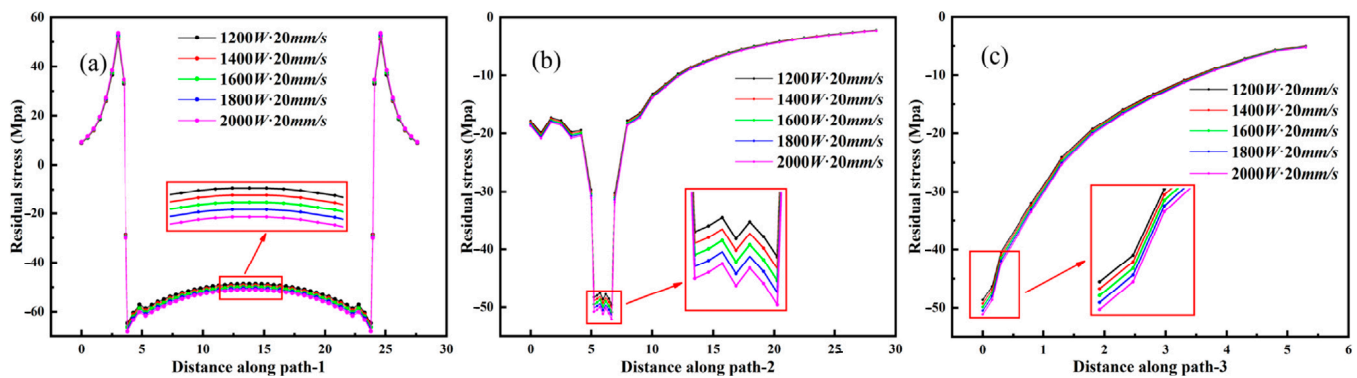


**Figure 6.** The distribution of residual stress under various laser power levels ((a) shows Path-1, (b) illustrates Path-2, and (c) represents Path-3 [61]).

Dubourg et al. [62] studied the mechanical properties of Al-Cu alloy coatings laser-alloyed onto the surface of pure aluminum. The results showed that when the Cu content was 40%, the hardness of the alloy was the highest, reaching  $250 \pm 10 \text{ HV}_{0.2}$ .

Table 1 presents the key findings for Al-based alloys. In summary, the use of Al-based alloys to address defects in aluminum alloy components has improved considerably. Leveraging Al-based materials can result in cost reductions. Nonetheless, challenges persist when using Al-based alloys as modification coatings. The degree of hardness enhancement achieved through such coatings is often limited, and while heat treatment might intensify surface hardness, it concurrently amplifies the residual stress within the coating. Moreover, even though the integration of ceramic materials can significantly augment hardness, potential issues related to coating cracking must be considered.

**Table 1.** Key findings on Al-based alloy coatings.

Authors	Coating Material	Key Findings
Meinert et al. [57]	4000 series Al	Repaired specimens had tensile strengths of 61% and 64% of their original counterparts.
Cottam et al. [58]	7075 Al	The cladding layer's hardness was 80% of the matrix. Heat treatment improved the hardness but also increased residual stress.
Corbin et al. [59]	6061-T6 Al	Coatings produced were without apparent defects. The cladding layer had coarser $\beta'$ precipitates with reduced hardness.
Dubourg et al. [62]	Al-Cu alloy	At 40% Cu content, alloy hardness peaked at $250 \pm 10 \text{ HV}_{0.2}$ .

## 2.2. Fe-Based Alloys

Fe-based alloy powders, with excellent wear resistance, low cost, and wide availability, have been used by some researchers for laser cladding onto the surface of aluminum alloys to improve surface wear resistance and anti-deformation.

Jeyaprakash et al. [63] used laser cladding technology to prepare a FeCrMoVC (H13 steel) cladding layer on the surface of an AA6061 aluminum alloy. The coating structure contained large carbides and martensite, the carbides formed by vanadium and molybdenum significantly improve the hardness of the coating. Compared with the base material, the wear resistance of the layer increased by nine times, and the surface roughness of the coating after wear was reduced by three times. Ye et al. [64] prepared a Fe-Al intermetallic compound cladding layer on the surface of ZL114A aluminum alloy. The microhardness of the cladding layer was as high as 614 HV, which is 5 to 6 times higher than the base material. Figure 7 shows the microstructure of the coating transition zone. Figure 7a illustrates the interface between the melt pool and the matrix, highlighting evident grain refinement in the transition

zone due to the rapid heating and cooling of the aluminum alloy surface. Figure 7b reveals the formation of dendritic grains along a specific growth direction at the bottom of the melt pool. In Figure 7c, these dendritic grains transform into equiaxial grains at the top of the melt pool. Cracks were found in the bonding zone, as shown in Figure 7d.

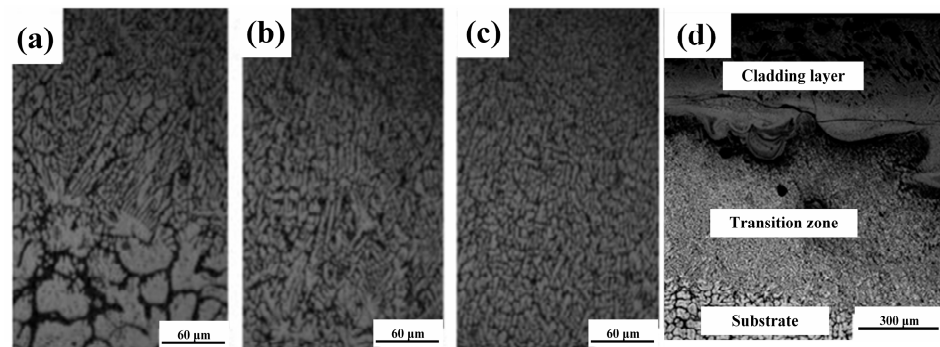


**Figure 7.** SEM images of the coating, (a) is the bottom of the transition zone, (b) is the middle of the transition zone, (c) is the top of the transition zone, and (d) is the macroscopic morphology of the bonding zone [64].

Tomida et al. [65] used a 2.2 kW continuous-wave CO<sub>2</sub> laser to prepare an xWt.%Al/Fe alloy coating on the surface of an A5052 aluminum alloy, including four Al-Fe mixed coatings with Al contents ranging from 10 wt.% to 40 wt.%. The results showed that the microstructure of the cladding layer consisted of  $\alpha$ -Al + FeAl<sub>3</sub>, FeAl<sub>3</sub>, and Fe<sub>2</sub>Al<sub>5</sub>, and the hardness reached 600–1000 HV. The alloy layers with fine needle-like FeAl<sub>3</sub> and Fe<sub>2</sub>Al<sub>5</sub> composite structures also have high hardness at a temperature of 673 K, 300 HV, and 800 HV, respectively. The wear resistance of such a coating is about 4–5 times higher than that of the aluminum alloy matrix. Mei et al. [66] found that the Fe-based coating prepared on the surface of an Al-Si alloy contained austenite, Cr<sub>7</sub>C<sub>3</sub>, and Cr<sub>23</sub>C<sub>6</sub>;  $\alpha$ -Al, NiAl<sub>3</sub>, Fe<sub>2</sub>Al<sub>5</sub>, and FeAl<sub>2</sub> were present at the junction; and  $\alpha$ -Al and Si were present in the heat-affected zone. Due to the generation of brittle intermetallic compounds, the coating was prone to cracking. Carroll et al. [67] performed the laser cladding of Fe powder prefabricated on the surface of a 319 aluminum alloy. The Al-Fe-Si intermetallic compound formed increased the hardness of the coating, but there was a significant increase in brittleness.

Table 2 presents the key findings for Fe-based alloys. In summary, using Fe-based alloy powder in laser cladding offers advantages like notable improvements in the mechanical properties of aluminum alloys and enhanced wear resistance at a low cost, but it also poses challenges. Specifically, Fe-based powder coatings on aluminum alloys can form various Fe-Al phase intermetallic compounds. This results in the frequent generation of defects such as pores and cracks in the bonding region, in addition to the challenges of pore formation in the cladding layer, limited enhancement in corrosion resistance, and the propensity for brittle intermetallic compounds. In response to these issues, future research may need to optimize cladding processes and alloy components further to improve the performance and stability of the coating.

### 2.3. Nickel-Based Alloys

Nickel-based alloys are known for their high hardness, wear resistance, corrosion resistance, and excellent resistance to high-temperature oxidation. They also have good wetting properties with aluminum substrates. Several advancements have been made in the laser cladding of aluminum alloys with nickel-based alloys.

**Table 2.** Key findings on Fe-based alloy coatings.

Authors	Coating Material	Key Findings
Jeyaprakash et al. [63]	FeCrMoVC	Coating has enhanced wear resistance; reduced surface roughness after wear.
Ye et al. [64]	Fe-Al intermetallic compound	Cladding layer has a hardness 5–6× that of the base material; cracks noted in bonding zone.
Tomida et al. [65]	Wt.%Al/Fe alloy (Al content: 10–40 wt.%)	The hardness of 600–1000 HV; wear resistance 4–5× greater than base matrix.
Mei et al. [66]	Fe-based coating	Contains multiple intermetallic compounds; prone to cracking due to brittle intermetallic compounds.
Carroll et al. [67]	Fe powder	Increased hardness with the Al-Fe-Si compound; significant increase in brittleness.

Wu et al. [68] applied a self-fluxing nickel-based powder coating to an  $\text{AlSi}_7\text{Mg}$  aluminum alloy surface via laser cladding. They found that different microstructures were formed in various regions of the coating. The top of the cladding layer consisted of a substantial amount of block- and network-shaped intermetallic compounds; the middle part had  $(\text{Ni}, \text{Cr}, \text{Fe})_x\text{C}_y$  intermetallic compounds. At the same time, columnar  $\alpha$ -Al dendrites with a distinct growth direction were prevalent at the bottom. The highest hardness, reaching 8200 MPa, was recorded in the top and middle parts of the coating. Adjusting the scanning speed could control the formation of pores and cracks in the coating.

He et al. [69] created a  $\text{TiB}_2$ -reinforced nickel-based composite coating on a 7005 aluminum alloy. The coating contained  $\text{NiAl}$ ,  $\text{Ni}_3\text{Al}$ ,  $\text{Al}_3\text{Ni}_2$ ,  $\text{TiB}_2$ ,  $\text{TiB}$ ,  $\text{TiC}$ ,  $\text{CrB}$ , and  $\text{Cr}_{23}\text{C}_6$  phases. Regarding the wear properties, a disk-type dry friction wear test was performed. Corundum, with a hardness of 9 on the Mons' scale, was the friction coupling, measuring  $\Phi 40 \text{ mm} \times 10 \text{ mm}$ . The wear samples were fashioned into 4.5 mm diameter and 10 mm height cylindrical shapes. The test was executed at a rotating speed of  $100 \text{ r} \cdot \text{min}^{-1}$ , subjected to a load of 20 N for 900 s. The hardness was 6.7 times that of the substrate, and the mass loss was reduced by up to 32.7%. As shown in Figure 8, the morphology of the  $\text{TiB}_2/\text{Ni}$ -based composite coating revealed that the powder was not fully melted, resulting in significant pore defects between particles.

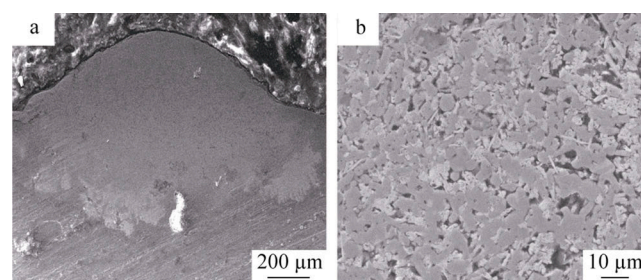


**Figure 8.** SEM of a cross-section of coating, (a) is the macroscopic morphology and (b) is the microstructure in the middle of the coating [69].

Liang et al. [70] prepared a  $\text{NiCrBSi}$  cladding layer on an Al-Si alloy surface using a  $\text{CO}_2$  laser. The cladding layer contained a large amount of  $\text{Ni}_3\text{Al}$ , with the highest microhardness reaching 1200 HV. In addition, by analyzing the aluminum–nickel eutectic system composition, they discovered that the solid solution formed by Cr, Si, and B with Al helped improve the resistance of the aluminum alloy to gas corrosion.

These studies suggest that forming aluminum–nickel intermetallic compounds can significantly enhance the hardness and wear resistance of coatings. However, the aluminum alloy substrate's and nickel-based cladding materials' physical and chemical properties differ greatly. As a result, defects such as cracks and pores can quickly form in the cladding layer. Relevant studies have shown that adding rare earth elements can alleviate this issue.

Wang et al. [71] added 5% rare earth elements to the Ni60 alloy during laser cladding on the surface of a 6063 aluminum alloy. They found that adding rare earth elements could improve the fluidity of the melt pool during the solidification process of the cladding layer and purify the melt pool. As shown in Figure 9, when only Ni60 alloy powder was used, many pores and cracks appeared in the cladding layer. After adding a certain amount of rare earth elements, the defects in the cladding layer, such as pores and cracks, were noticeably improved. After adding rare earth elements, the cladding layer's structure was refined, with no apparent pores or segregation.

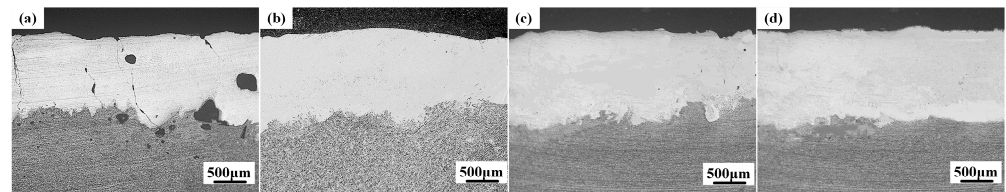


**Figure 9.** SEM of a cross-section of coatings, (a) is Ni60, (b) is  $\text{La}_2\text{O}_3 + \text{Ni60}$ , (c) is  $\text{Y}_2\text{O}_3 + \text{Ni60}$ , and (d) is  $\text{CeO}_2 + \text{Ni60}$  [71].

Zhang et al. [72] prepared a nickel-based cladding layer with a nickel–copper ratio of 4:1 on the surface of a 6061 aluminum alloy. They added a certain proportion of rare earth  $\text{CeO}_2$ , Si, and Co powders to the cladding powder. The top of the coating was primarily composed of equiaxed crystals, dendrites, and tiny equiaxed crystals, while the bottom of the cladding layer was mainly composed of long rod-shaped crystals, dendrites, and some particles. After adding  $\text{CeO}_2$ , Si, and Co powders into the cladding materials, the cladding layer's hardness increased, and the average friction factor decreased, thanks to the grain refinement of  $\text{CeO}_2$  and the dispersion strengthening effect of Si and Co in the coating. Figure 10 portrays the microstructural variances across the top and bottom regions of Ni-Cu,  $\text{CeO}_2/\text{Ni-Cu}$ , Si/Ni-Cu, and Co/Ni-Cu composite coatings. Specifically, Figure 10a,b demonstrate the microstructure of the top and bottom regions in a 100 wt.% M coating, wherein the top area is primarily populated by grey rod-like and equiaxed grains. The bottom zone, conversely, presents a different structure. Figure 10j,k extend this analysis to the Co/M coating, revealing that the top region predominantly comprises short dendritic phases. Figure 10d–f illustrate the microstructure when the base metal is alloyed with 0.9 wt.% of cerium oxide ( $\text{CeO}_2$ ), resulting in a composition that is 99.1 wt.% M and 0.9 wt.%  $\text{CeO}_2$ . This minor addition of  $\text{CeO}_2$  is intended to investigate the effects of rare earth oxide inclusion on the microstructure. Figure 10g–i display the coatings where silicon (Si) has been added at 0.9 wt.%, making up a total composition of 99.1 wt.% M with the inclusion of silicon. This variation is aimed at understanding the influence of Si on the microstructural characteristics of the coating. The corresponding XRD results, illustrated in Figure 10c,l, corroborate these structural characterizations. These findings underscore the significant microstructural differences between the top and bottom regions across various composite coatings.

Table 3 presents the key findings for Ni-based alloys. Current domestic and international research shows that with the use of a laser heat source, the temperature field distribution of the melt pool is uneven, leading to different structures at the top and bottom of the cladding layer. Nickel-based alloys, especially when modified with Ni-based materials as the coating, have good compatibility with the aluminum substrate. The intermetallic compounds formed by Ni and Al not only improve the hardness of the cladding layer but also significantly increase its brittleness. Introducing rare earth oxides in a Ni-based coating material can enhance the quality of the formed layers, and this approach has garnered attention as a method for improving the coating's formation quality. However, there is a critical consideration: the melting point of many rare earth oxides surpasses the boiling point of aluminum alloys. In producing superior coatings, the laser heat input must achieve a delicate balance—sufficient to melt the added powder thoroughly but without overly diluting or evaporating the substrate. This challenge narrows the range of acceptable

process parameters for laser deposition when incorporating high-melting-point rare earth oxides, increasing the influence of system errors on the coating quality during experimentation. Achieving a uniform microstructure, refined grains, and reasonably controlling the formation of brittle and hard phases is critical to the laser cladding of nickel-based alloys on the surface of aluminum alloys. Simultaneously, while the inclusion of rare earth elements can notably enhance the quality of the formed coatings and diminish their sensitivity to cracking, the elevated costs and high melting point characteristics associated with these elements necessitate technological advancements to mitigate these issues when applying nickel-based coatings in aluminum alloy surface cladding.

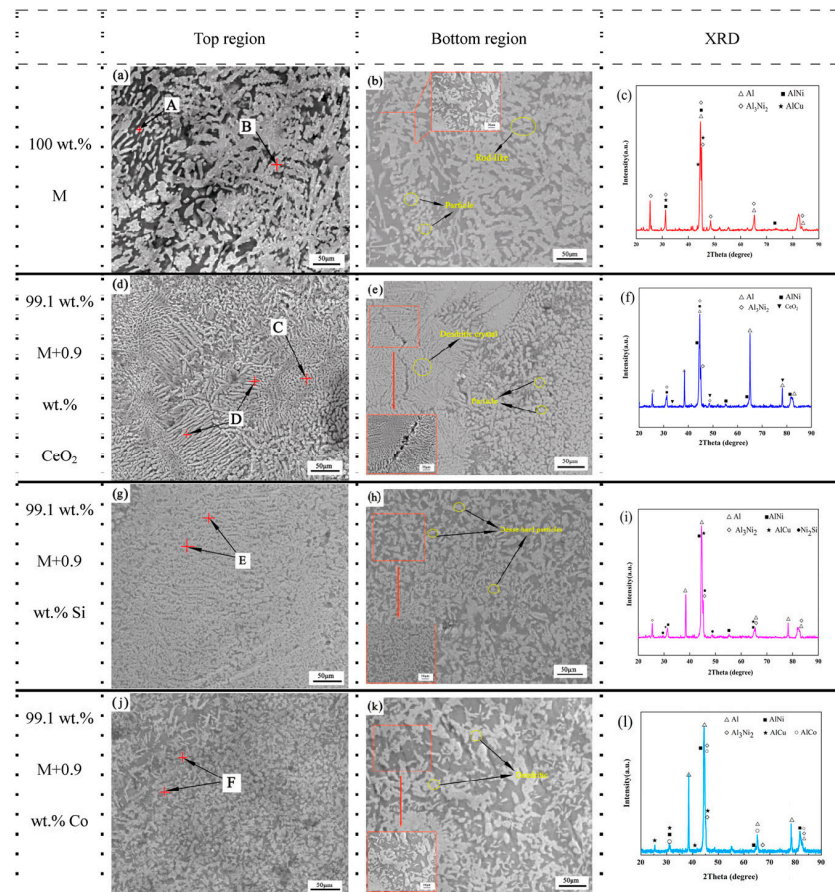


**Figure 10.** Characteristic microstructures of cladding coatings across different compositions. (a–c) is 100% wt. M (d–f) is 99.1% wt.%M + 0.9 wt.% CeO<sub>2</sub> (g–i) is 99.1% wt.%M + 0.9 wt.% Si (j–l) is 99.1% wt.%M + 0.9 wt.% Co [72].

**Table 3.** Key findings on Ni-based alloy coatings.

Authors	Coating Material	Key Findings
Wu et al. [68]	Nickel-based alloy	Microstructure variations; peak hardness at 8200 MPa; effect of speed on defects
He et al. [69]	TiB <sub>2</sub> -reinforced nickel-based composite	Coating hardness 6.7× substrate; mass loss reduced by 32.7%; notable pore defects.
Tan et al. [73]	Nickel-based alloy	Enhanced coating hardness and wear resistance compared to substrate.

Table 3. Cont.

Authors	Coating Material	Key Findings
Liang et al. [70]	NiCrBSi	Cladding contains Ni <sub>3</sub> Al with a peak microhardness of 1200 HV.
Wang et al. [71]	Ni60 alloy with 5% rare earth elements	Rare earth elements improved coating structure and reduced defects.
Zhang et al. [72]	Nickel-based (Ni-Cu ratio of 4:1) with CeO <sub>2</sub> , Si, and Co	Additives (CeO <sub>2</sub> , Si, Co) improved coating hardness and reduced friction.

### 3. Ceramic-Reinforced Composite Coating

Ceramics, with their high hardness, high melting point, and excellent wear resistance, are widely acknowledged as suitable materials for laser cladding. Adding ceramic particles to metal-based laser cladding materials can exploit the non-linear superimposed effects of their physical properties between the ceramic reinforcement phase and the metal matrix. Combining the excellent toughness and machinability of the metal matrix with the high hardness and wear resistance of the ceramic reinforcement phase can enhance the surface of the base material. In laser cladding on the surface of aluminum alloys, ceramic phases are commonly used as reinforcement, added to the metal-based composite materials. These ceramic phases include carbide ceramics, such as WC, SiC, TiC, oxide, nitride, and boride.

Sun et al. [74] via laser cladding, prepared a SiC/Al-12Si composite coating on the surface of an Al-12Si aluminum alloy substrate. Studies have found that the layer and the substrate are divided, and the organization of the bonding area is mainly composed of  $\alpha$ -Al dendrites, a small amount of Al-Si eutectic, and a small number of SiC particles. In contrast to the base material, the hardness of the cladding layer increased by about two times, reaching approximately 260 HV<sub>0.2</sub>.

Anandkumar et al. [75] prepared a 12 wt.%TiB<sub>2</sub>/Al-based composite coating on the surface of a 7 wt.%Si/Al casting aluminum alloy via laser cladding. To assess the wear performance of the prepared cladding, microscale abrasive wear tests were conducted using a ball cratering device. The abrasive medium for these tests was a suspension containing 35 wt.% SiC particles (with an average diameter of 4.25  $\mu$ m) in water. The counter body, which rotates against the sample's surface during testing, was a 19 mm diameter sphere made of quenched and tempered AISI 440C tool steel, boasting a hardness of 800 HV. The tests employed a uniform sliding distance of 150 m and exerted a regular load of 0.1 N. The cladding layer mainly consisted of  $\alpha$ -Al dendrites and  $\alpha$ -Al-Si eutectic, with a micro-hardness of 156 HV<sub>0.2</sub>, an approximately 1.7 times increase compared to the base material. Figure 11 illustrates that the microstructure of the deposited material is highly dependent on the laser processing parameters. A cladding prepared with a power density of 330 W/m<sup>2</sup> and a brief interaction time of 0.08 s—corresponding to a specific energy of 26 J/m<sup>2</sup>—exhibits a microstructure primarily composed of SiC particles dispersed within an aluminum alloy matrix, as shown in Figure 11a. This matrix comprises primarily  $\alpha$ -Al dendrites and an  $\alpha$ -Al+Si eutectic, as shown in Figure 11d. The volume fraction of SiC stands at 28  $\pm$  3%. The TiB<sub>2</sub> reinforcement phase in the coating effectively protected it, enhancing its wear resistance and reducing its sliding friction coefficient to 2.65  $\times$  10<sup>-5</sup> mm<sup>3</sup>/(N·m), approximately 2.4 times lower than the base material.

They [76] also laser clad a mixture of Al-12%Si and TiC ceramic particles on the surface of Al-7%Si casting aluminum alloy, successfully obtaining a cladding layer with no apparent defects. The cladding layer mainly contains uniformly distributed TiC particles, interdendritic  $\alpha$ -Al+Si eutectic, dendritic  $\alpha$ -Al, and a small amount of Ti<sub>3</sub>SiC<sub>2</sub>, indicating the partial dissolution of TiC particles. The cladding layer's friction coefficient decreased 2–3 times compared to the base material. Only a small amount of Al and Si were found in the worn-off material from the base material's surface, with no TiC particles detected.

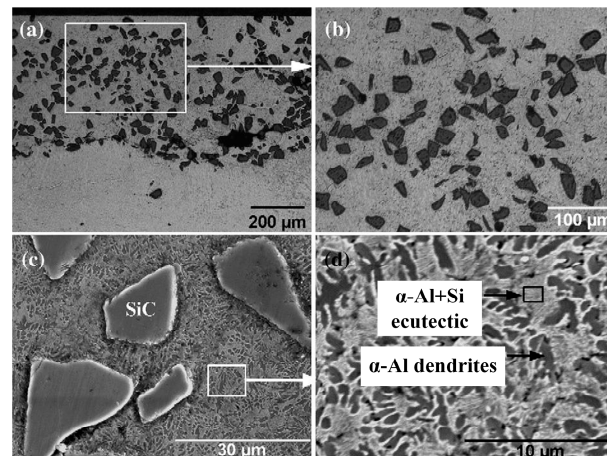


**Figure 11.** Microscopic illustrations of a coating formulated utilizing a power density of  $330 \text{ MW/m}^2$  and a contact period of 0.08 s. (a) is a transversal representation of the layer; (b,c) are SiC particles scattered in the matrix; and (d) is the intricate design of the matrix at a microscopic level [75].

Liu et al. [77] prepared an Al-Si-based composite layer reinforced with SiC particles on a 4032 aluminum alloy. Chemical copper plating improved the wettability between SiC and the substrate, while increasing the SiC content within a specific range can reduce the cladding layer's wear.

Li et al. [78] prepared a Ti/TiBCN coating on the surface of a 7075 aluminum alloy using laser cladding. To evaluate the wear resistance of the cladding coatings, tests were conducted using an MFT-R4000 straight-line-reciprocating dry sliding wear tester at room temperature without any lubrication. The test parameters were set at a normal load of 5 N, a friction distance of 5 mm, a frequency of 2 Hz, and a sliding duration of 20 min. The counterpart material for the friction test was GCr15 steel (5 mm in diameter), with a macro-hardness of HRC65. Figure 12 presents a detailed look at the microstructures in various zones. Figure 12a,b reveal the microstructure of the coating zone, composed primarily of equiaxed grains and uniformly dispersed white lath-like crystals. Figure 12c,d portray the transition zone's microstructure, notable for its sudden shift from equiaxed grains to an elongated structure filled with small white particles. Figure 12e,f depict the heat-affected zone's microstructure, characterized by a transverse equiaxed crystal structure resulting from the effects of rapid heating and cooling. The average hardness of the coating is  $519.4 \text{ HV}_{0.2}$ , 4.3 times that of the base material; the average friction coefficient of the layer is 0.208, half that of the base material. Compared with solely Ti powder cladding, adding a certain proportion of TiBCN ceramics to the cladding material can further enhance the coating's wear resistance and corrosion resistance. When the TiBCN content is 15%, the wear and corrosion opposition reach their best.

He et al. [69] prepared a Ni-based alloy composite coating reinforced with  $\text{TiB}_2$  ceramic particles on the surface of a 7005 aluminum alloy to enhance the wear resistance of aluminum alloy friction components. Tribological assessments were conducted using an HT-500 ball-on-disk tribometer, where specimens slid against a GCr15 ball ( $U = 4 \text{ mm}$ ) under varied loads of 3, 6, 9, and 12 N at a steady speed of  $0.5 \text{ m}\cdot\text{s}^{-1}$  for 500 m, conducted at  $20^\circ\text{C}$ . The micro-hardness of this ceramic-reinforced composite material cladding layer is  $855.8 \text{ HV}_{0.5}$ , 15.4% higher than the Ni-based alloy coating and 6.7 times that of the aluminum alloy substrate.

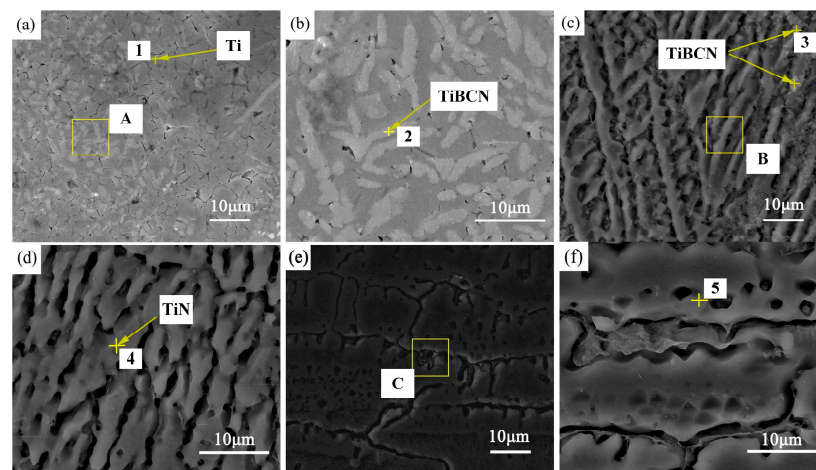


**Figure 12.** Distinctive cross-sectional microstructures within different zones of the cladding coating prepared with 15 wt.% TiBCN powder. (a) is the uppermost layer of the cladding coating. (b) is a magnified snapshot of quadrangle [A] in (a). (c) is the transition zone. (d) is a magnified view of the quadrangle in (c). (e) is the heat-affected zone. (f) is an enlarged depiction of the quadrangle in (e) [78].

The poor ductility, small elastic modulus, low thermal conductivity, and high melting point of ceramic materials can lead to cracks, deformation, and delamination in the cladding layer. Therefore, research on cladding a single ceramic onto the surface of an aluminum alloy is relatively scarce, and composite cladding layers of ceramic-reinforced materials mixed with metal materials are typically prepared. To address the challenges of laser cladding ceramic materials on aluminum alloys, solutions can be sought from the perspectives of optimizing process parameters, controlling the composition of cladding materials, improving powder properties, adding appropriate transition layers, and the in situ generation of ceramic reinforcement phases.

Regarding the control of the cladding material composition, Riquelme et al. [79] aimed to address the issue of harmful  $Al_4C_3$  compound formation during the laser cladding of a SiCp-reinforced Al-based composite coating on an aluminum alloy surface. They manipulated the reaction equilibrium of  $Al_4C_3$  by adding different alloy elements, thereby preventing the formation of  $Al_4C_3$ . When the Si content was low, needle-shaped  $Al_4C_3$  appeared in the cladding layer. When the Si content exceeded 40 wt.%, the appearance of  $Al_4C_3$  was entirely inhibited, and more SiC particles were observed, significantly improving the hardness of the cladding layer.

In terms of the improvement of powder properties, Kamaal et al. [80] addressed the issue of limited cladding efficiency due to the high reflectivity of aluminum alloys and the difficulty with ceramic material cladding. They studied the impact of powder satellite technology on the cladding of Al-TiC powder on a 6082-T6 aluminum alloy substrate. The hardness and wear performance of the specimens were then assessed. The wear performance of these samples was evaluated using a CETR Universal Micro-Tribometer 3, following the ASTM G133-05 standard [81]. Tests were conducted over 10 min, using a 5 mm displacement amplitude at 1 Hz frequency. An AISI steel ball (grade 440 C, 800 HV, 6 mm diameter) was the counter body under a 5 N load. The top surfaces of the claddings, post grinding to their center, were the focus of these tests.

In the satellite technology employed in that study, the Al-TiC powder mixture underwent both dry and wet mixing processes. A binder was sprayed over the mixed powder to achieve a uniform distribution. Subsequent mixing steps ensured the homogeneous distribution of the components, breaking down any potential agglomerations or clusters. After mixing, the satellited powder was dried, evaporating the water content and leaving behind only a minuscule percentage of the binder. This method aims to obtain a better homogenized powder feedstock, ensuring the consistent distribution of its components.

Compared with the directly mixed cladding material, the cladding efficiency and TiC content in the cladding layer increased by 29% and 113%, respectively, after using satellite technology. Figure 13 shows the cross-sectional images of the directly mixed powder and satellite powder cladding layer. As can be seen, the cladding material after using satellite technology resulted in better formation of the cladding layer, with more TiC content and a more uniform distribution. The microhardness measurements for blended and satellited claddings were created at different laser densities. The average microhardness for the combined class lies between 37.7 and 51.6 HV<sub>0.025</sub>. Claddings produced at 104 and 122 J/mm<sup>2</sup> have similar hardness values. A slight increase in hardness from 104 to 122 J/mm<sup>2</sup> is linked to denser structures and an 83% decrease in porosity at the higher laser density. The average micro-hardness of the cladding layer improved by 60%, and the wear rate decreased by 64%.

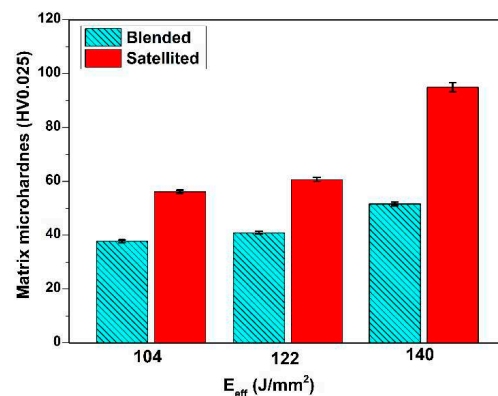


**Figure 13.** The microhardness measurements of blended and satellited cladding matrices generated at assorted  $E_{eff}$  values [80].

Table 4 presents the key findings for ceramic-reinforced composites. In general, due to their inherent high hardness and exceptional wear resistance, ceramics significantly enhance the cladding layer's hardness when applied to aluminum alloy surfaces. Introducing ceramic particles into metal-based laser cladding materials can produce a synergistic effect between the ceramic reinforcing phase and the metal matrix. This synergy results in a composite coating that combines high strength with flexibility. Regarding material selection, various ceramics such as WC, SiC, TiC, and others like oxides, nitrides, and borides can be used as reinforcing materials, providing a diverse array of choices tailored to specific applications. For instance, coatings enriched with TiBCN have showcased superior corrosion resistance. However, ceramic laser cladding on aluminum alloys comes with its challenges. Given the high hardness and brittleness of ceramics, coating cracking is a potential risk. Ensuring a strong metallurgical bond between the ceramic phase and the aluminum alloy substrate is paramount, especially considering the non-metallic nature of ceramics. Additionally, the microstructure of the ceramic material can be highly influenced by laser processing parameters, emphasizing the importance of optimal parameter selection to achieve the desired outcome. Finally, from a financial standpoint, the cost of employing high-quality ceramics should be taken into account, as it might have implications on the overall economic feasibility of a project.

**Table 4.** Key findings on ceramic-reinforced composite coatings.

Authors	Coating Material	Key Findings
Sun et al. [74]	SiC/Al-12Si composite	Doubled the hardness of the cladding layer to approximately 260 HV <sub>0.2</sub> .
YANG et al. [77]	Al-Si-based composite with SiC	Wear resistance of cladding layer increased.
Li et al. [78]	Ti/TiBCN	Coating's hardness 4.3 times higher than base material; reduced friction coefficient.
Kamaal et al. [80]	SiC-reinforced Al-based	Achieved improved hardness by preventing Al <sub>4</sub> C <sub>3</sub> formation.

#### 4. Emerging Coatings

Currently, the emerging material coatings studied for laser cladding on the surface of aluminum alloys primarily include amorphous alloys and high-entropy alloys (HEAs).

##### 4.1. Amorphous Materials

The traditional alloy cladding materials significantly differ from aluminum substrates in terms of properties, resulting in an increased difficulty with and reduced effectiveness of laser cladding on aluminum alloys. Table 5 shows the mixing enthalpy, melting point, and specific gravity of Al elements and some metal cladding materials [81]. It can be seen that the mixing enthalpy of aluminum elements with other metal elements is relatively small. The aluminum substrate has a low melting point and high dilution rate, and the lower-density aluminum elements in the substrate can easily transition to the cladding layer and form brittle compound phases with features in the cladding layer, increasing the tendency for cracking in the cladding layer. If the design of cladding materials could consider the characteristics of rapid heating and cooling in laser cladding and prepare cladding layers that are less prone to brittle phases, that would be the first new attempt and exploration in the field of laser cladding in recent years. Currently, the emerging material coatings studied for laser cladding on the surface of aluminum alloys primarily include amorphous alloys and high-entropy alloys

**Table 5.** Thermal properties of typical transition metals: mixing enthalpy, melting point, and specific weight [81].

	Fe	Cr	Ni	Co	Cu	Al
Mixing Enthalpy with Al (kJ/mol)	−11	−10	−22	−19	−1	-
Melting Point (°C)	1538	1857	1455	1495	1083	660
Specific Weight	7.89	7.19	8.9	8.9	8.96	2.6

Amorphous alloys, which have long-range disordered and short-range ordered structures similar to glass, are formed by inhibiting nucleation during the solidification of molten materials. They lack crystal defects such as vacancies, dislocations, and stacking faults and therefore possess advantages such as high hardness, wear resistance, and corrosion resistance. The fast cooling rate of laser cladding makes it possible to apply amorphous materials to laser cladding [82–86].

Sohrabi et al. [87] prepared Zr-based amorphous cladding layers on an AA2011-T6 aluminum alloy surface and studied the relationship between the coating crystallization rate and thermal input. The cladding layers produced under higher laser power yielded more diffraction peaks than other samples. Reducing the energy density can inhibit crystal crystallization. For samples with a laser power of 35 W and overlapping distance of 95 μm, the obtained cladding layer appears amorphous under the detection resolution of XRD tests. The wear resistance of the Zr-based amorphous cladding layer is 20 times that of the aluminum alloy substrate. Figure 14a displays a SEM examination of the wear

track for a sample created with optimized parameters, leading to 1% crystallization. This wear evaluation was conducted under specific test conditions to ensure a comprehensive understanding of the material's behavior. Wear tests were conducted on the surface of the samples, which were polished down to a sandpaper with a 2500 mesh size, using a reciprocating tribometer in a ball-on-flat configuration.  $\text{Al}_2\text{O}_3$  balls with a diameter of 6 mm served as the counterpart. During the test, an applied normal force of 2 N was maintained at an average speed of 6 mm/s and a 1 Hz frequency. Each trial lasted 30 min, with a stroke length of 3 mm, culminating in a total sliding distance of 10.8 m. Precautions were taken to clean the sample surfaces and the counterpart balls in ultrasound baths with acetone, followed by ethanol, and they were then dried with oil-free compressed air.

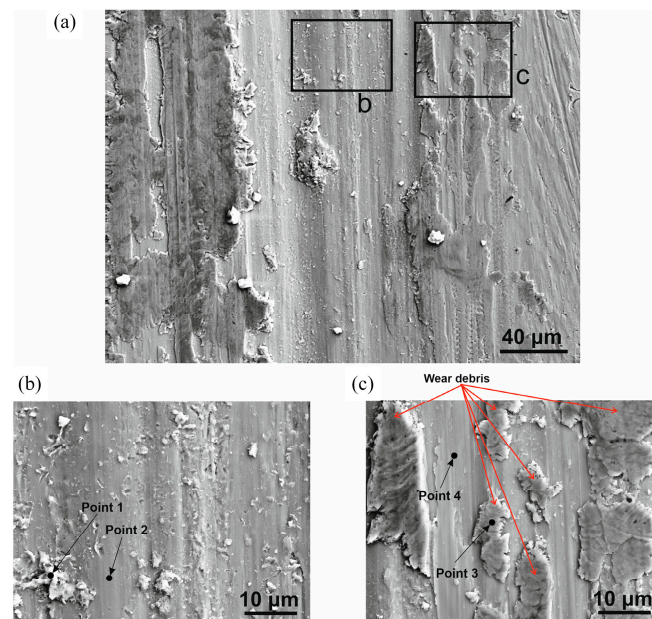


**Figure 14.** (a) SEM micrograph of the wear track (b) magnified image of region B in (a), and (c) magnified image of region C in (a) [87].

Figure 14b,c give detailed views of regions b and c. Wear debris is spotted at Points 1 and 3, while Points 2 and 4 represent the areas with preserved coating. The oxygen at Points 1 and 3 is likely due to the wear debris interacting with air. The observed wear patterns and debris suggest a wear mechanism that is a combination of abrasive and oxidation wear.

The formation of amorphous materials is related to the ratio of material components, and obtaining high-quality amorphous cladding layers requires preventing segregation in the coating. Wang et al. [88] used a fiber laser to clad an Al-Ni-Y ternary alloy powder onto a ZL114 aluminum alloy surface to study its ability to form amorphous coatings on aluminum alloys via laser cladding. The cladding layer mainly comprised blocky dark areas and fewer net-like bright areas. The bright regions contained more Ni and Y elements, while the dark spots contained less Ni and Y. The atomic ratio of elements in the bright grain boundary areas is close to  $\text{Al}_{85.8}\text{Ni}_{9.1}\text{Y}_{5.1}$ , which has the strongest ability to form amorphous alloys in the Al-Ni-Y system. However, XRD results did not show the apparent complete reflection of the amorphous alloy, indicating that there are still some difficulties in preparing amorphous coatings on the aluminum alloy surface via laser cladding under these experimental conditions. The Ni and Y transition issue in the cladding layer must be resolved.

Table 6 presents the key findings for amorphous coatings. As a novel coating material, current research on applying amorphous coatings to aluminum alloy surfaces remains limited. However, such coatings can significantly enhance the substrate's corrosion and wear resistance. Precise control over processing parameters and material composition ratios

is vital to prevent segregation within the coating. Delving deeper into optimizing these amorphous coatings' structures, organization, and performances through laser cladding is still a topic warranting further investigation.

**Table 6.** Key findings on amorphous coatings.

Authors	Coating Material	Key Findings
Sohrabi et al. [87]	Zr-based amorphous	Coating's wear resistance is 20× that of the substrate; reduced energy density inhibits crystallization.
Wang et al. [88]	Al-Ni-Y ternary alloy powder	Bright regions of the layer contain more Ni and Y; challenges in achieving fully amorphous coatings.

#### 4.2. High-Entropy Alloys

In traditional metallurgy, one or two elements are usually selected as the main components of alloy design, with a small number of other elements added to adjust alloy properties. Only a tiny fraction of the given material can be changed. This imposes a significant constraint on the combination of elements, making it challenging to improve traditional materials or develop new ones. Many application fields are not adequately catered for, especially where hardness and wear resistance are paramount. Greer's "Confusion Principle" suggests that an excess of elements would make it difficult for an alloy to maintain its crystalline state, leaning more towards an amorphous state. Due to this, traditional alloy design struggles to break free from the shackles of single-element design. The emergence of HEA, a new material system, breaks this classic alloy design pattern, opening up a new direction for alloy design in materials science [89–95].

HEAs comprise five or more elements in equal atomic ratios. In recent years, scholars have expanded the concept of HEA to include 3 or 4, but fewer than 13, primary elements, with each element's concentration ranging from 5 at% to 35 at% [96–99]. According to traditional metallurgy theories, multi-principal element alloys such as HEAs would generate complex intermetallic compounds (IMCs). However, due to the high configurational entropy of HEAs, simple solid-solution phases become the main phase structures of HEAs, such as Face-Centered Cubic (FCC), Body-Centered Cubic (BCC), and Hexagonal Close-Packed (HCP) structures [64,98,100–107]. The difficulty in preparing aluminum alloy coatings lies in inhibiting the formation of hard and brittle phases caused by substrate dilution behavior and ensuring excellent coating performance. The four core effects of high-entropy alloys provide a theoretical basis for solving this problem.

Shon et al. [108] used a two-step thermal spray–laser cladding process to prepare AlCrFeCoNi HEAs on the surface of a 1100 aluminum alloy in situ, having found that the high-energy density multi-layer cladding process could reduce defects like coating porosity and cracking. They discovered that the high-energy density multi-layer cladding process could significantly minimize defects such as coating porosity and cracking. An essential factor in this process is the energy density, given by the formula  $E = P / (v \times w)$ , where  $E$  is the energy density ( $J/mm^2$ ),  $P$  is the laser power (W),  $v$  is the scanning speed (mm/s), and  $w$  is the beam width (mm). This energy density is pivotal as it governs the melting behavior and the dilution between the coating and substrate. The energy density plays a crucial role in determining the dilution rate of the coating. When the energy density is high, the substrate elements are more diffused into the coating, leading to a deviation from the coating's initial compositional ratio. Conversely, at lower energy densities, the diffusion from the substrate is limited, allowing the coating to maintain its original compositional balance.

Figure 15a represents various samples' corrosion rates (color) and corrosion potentials ( $E_{corr}$ ) extracted from potentiodynamic polarization curves. Although the  $E_{corr}$  values remain similar across models, there are significant differences in the  $i_{corr}$  values. Figure 15b reveals the extensive pitting corrosion in the untreated Al1100 sample. Figure 15c shows the corroded surface of the single-layered coating processed at  $21 J/mm^2$ . It exhibits sub-

stantial corrosion, predominantly in pitting and surface cracking. There are also signs of micro-galvanic corrosion. Figure 15d illustrates the corroded surface of a double-layered sample processed at 21 J/mm<sup>2</sup>. Although minor pitting is observed, it is highly localized, indicating a homogenous composition and microstructure. Figure 15e shows a double-layered sample processed at 25 J/mm<sup>2</sup>, which experienced minimal or no pitting corrosion. This demonstrates the benefits of minimized compositional dilution and uniform distribution of the high-entropy alloy phase. Different processing conditions affected the microstructure and subsequent corrosion behavior of the materials. Single-layer samples at 21 J/mm<sup>2</sup> exhibited lower corrosion resistance than double-layered samples due to a more heterogeneous structure and substantial substrate dilution. This caused an increase in corrosion rate.

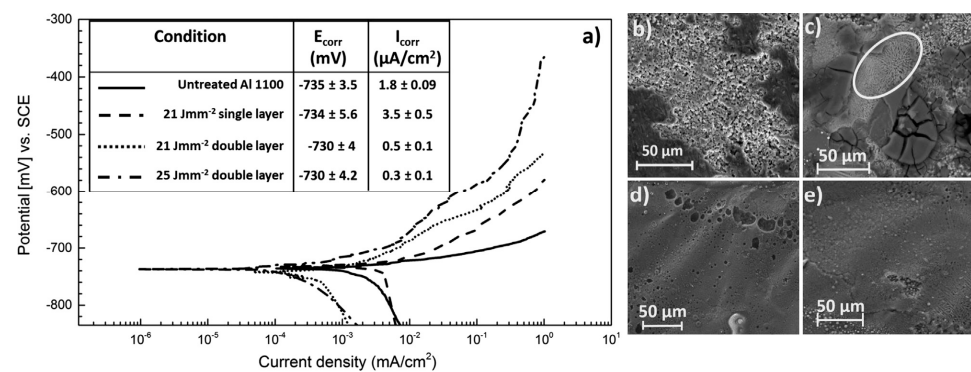


**Figure 15.** The corrosion results for the HEA coatings (a) is a cyclic polarization diagram for the coatings and Al1100 substrate, (b) is the corroded surface micrographs for untreated Al1100 substrate, (c) is 21 J/mm<sup>2</sup> single HEA layer, (d) is 21 J/mm<sup>2</sup> double HEA layer and (e) is 25 J/mm<sup>2</sup> double layer [108].

In contrast, double-layered samples showed improved corrosion resistance, particularly at a processing intensity of 25 J/mm<sup>2</sup>, which exhibited minimal or no pitting corrosion. This was attributed to reduced compositional dilution and a uniform high-entropy alloy phase. The system benefited from corrosion-resistant elements and a lower aluminum content.

Siddiqui et al. [109] surface-modified an aluminum substrate with mixed powders of high-purity Cu, Fe, Ni, and Ti, and the Al<sub>x</sub>Cu<sub>0.5</sub>FeNiTi HEA coating displayed a mixture of two FCC solid solutions and disordered BCC, with hardness reaching 18 times that of the substrate.

Ye et al. [110] laser-clad an Al<sub>x</sub>FeCoNiCuCr HEA coating on the surface of an aluminum alloy. As the Al content increased from 1 to 2, the hardness increased from 390 to 687 HV<sub>0.2</sub>. Li et al. laser-clad a Ti<sub>x</sub>CrFeCoNiCu HEA coating on the surface of an aluminum alloy. Wear tests were conducted under ambient conditions, utilizing a GCr15 steel ring with a hardness of 61 HRC as the counter material. This ring measured 50 mm in diameter and 10 mm in thickness. The test samples had dimensions of 7 × 14 × 10 mm. Under a 98 N load and at 40 r/min, the experiments lasted for 30 min. Subsequently, the wear rate was determined from the evaluated wear volume. As the Ti content increased, the phase structure of the Ti<sub>x</sub>CrFeCoNiCu coating changed from a single FCC to FCC + B2 phase and FCC + Laves phase, and the hardness increased from 215 HV<sub>0.2</sub> to 585 HV<sub>0.2</sub>. The addition of Ti significantly improved the wear resistance of the coating. Ma et al. [111] added equal moles of Cu and Ti to FeCoNiCr HEA powder to improve the performance of a 6061 aluminum alloy. The coating had high hardness and wear resistance due to the synergistic effect of solid solution strengthening, dispersion strengthening, and grain refinement. Shi et al. [27,112,113] prepared an AlCrFeNiCuCoCu system HEA coating on a 5083 aluminum alloy. The coating consisted of FCC + BCC and Al-rich phases, with higher hardness and corrosion resistance than the substrate.

Li et al. [114] explored the use of  $\text{Al}_{0.8}\text{FeCoNiCrCu}_{0.5}\text{Si}_x$  ( $x$  ranges from 0 to 0.5) HEAs as cladding materials. They harnessed the unique high-entropy impact of HEAs to limit the development of hard, brittle intermetallic compounds, enhancing the coating's quality and thereby upgrading the surface attributes of the Al alloy. The wear tests were conducted at room temperature, using a GCr15 steel ring as the counter material, which has a hardness of 61 HRC. The steel ring had a diameter of 50 mm and a thickness of 10 mm, while the wear sample dimensions were  $7 \times 14 \times 10$  mm. The tests were performed under a load of 98 N and at a speed of 40 r/min for 30 min. The wear rate of the material was deduced from the calculated wear volume. These specific testing conditions ensure that the wear behavior of the HEA claddings is understood within a defined operational environment.

As the Si content increased, the structure of the  $\text{Al}_{0.8}\text{FeCoNiCrCu}_{0.5}\text{Si}_x$  coating shifted from FCC + BCC1 + BCC2 to a solely BCC1 + BCC2 formation. The hardness of the  $\text{Al}_{0.8}\text{FeCoNiCrCu}_{0.5}\text{Si}_x$  coating initially rose, then fell as the Si content increased. The most and least hard coatings were those composed of  $\text{Al}_{0.8}\text{FeCoNiCrCu}_{0.5}\text{Si}_{0.4}$  (592  $\text{HV}_{0.2}$ ) and  $\text{Al}_{0.8}\text{FeCoNiCrCu}_{0.5}$  (412  $\text{HV}_{0.2}$ ), respectively, representing hardness levels five to seven times that of the substrate. The Si content influenced the wear resistance of the coating similarly to its effect on hardness. With different Si contents, the wear rates ranged from  $1.19 \times 10^{-6} \text{ mm}^3/\text{Nm}$  to  $8.99 \times 10^{-7} \text{ mm}^3/\text{Nm}$ , constituting only 0.25% to 0.34% of the substrate's rate. Figure 16a presents the wear surface of an Al alloy, which is characterized by severe plastic deformation along the wear direction, elongated dimples, and a stepped fracture. Figure 16b shows the  $\text{Si}_0$  coating's wear surface, displaying a peeling surface, furrow, and fine abrasive particles. The  $\text{Si}_{0.2}$  coating's wear surface in Figure 16c shows similar features to the  $\text{Si}_0$  coating. The wear surfaces of  $\text{Si}_{0.3}$  and  $\text{Si}_{0.4}$  coatings in Figure 16d,e, respectively, exhibit a disappearance of the peeling surface and a predominance of abrasive particles. Among them, the  $\text{Si}_{0.4}$  coating presents fewer abrasive particles and a shallower furrow, suggesting better wear resistance. Finally, in Figure 16f, the wear surface of the  $\text{Si}_{0.5}$  coating is featured, showing the distribution of an adhesion layer and furrow interval.

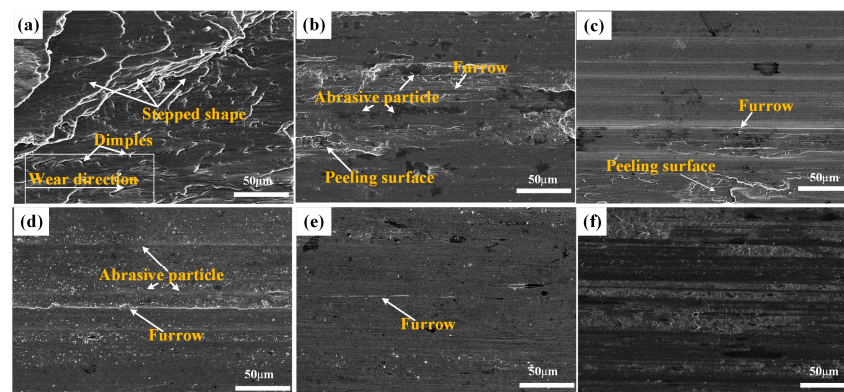


**Figure 16.** Wear surface morphology of samples; (a) is 5083 aluminum alloy; (b) is  $\text{Al}_{0.8}\text{FeCoNiCrCu}_{0.5}\text{Si}$ ; (c) is  $\text{Al}_{0.8}\text{FeCoNiCrCu}_{0.5}\text{Si}_{0.2}$ ; (d) is  $\text{Al}_{0.8}\text{FeCoNiCrCu}_{0.5}\text{Si}_{0.3}$ ; and (e) is  $\text{Al}_{0.8}\text{FeCoNiCrCu}_{0.5}\text{Si}_{0.4}$ ; (f) is  $\text{Al}_{0.8}\text{FeCoNiCrCu}_{0.5}\text{Si}_{0.5}$  [114].

Table 7 presents the key findings for HEA coatings. Due to their high mixing entropy, HEAs have high degrees of disorder at room temperature, which increases with temperature. According to Gibbs's free energy, the larger the entropy, the smaller the system's free energy and the more stable the system. The high mixing entropy of HEAs significantly reduces their free energy, thereby reducing the trend of order during solidification, inhibiting the generation of intergranular compounds, promoting the formation of solid solutions, and resulting in coatings with more stable crystal structures. When applied to the surface of aluminum alloys, these coatings exhibit excellent mechanical properties and corrosion resistance. However, the industrial application of high-entropy

alloys with high melting points and high costs still needs further exploration. However, given aluminum's low melting point, current laser cladding HEA coatings on aluminum alloy surfaces predominantly focus on the FeCoNiCrCu system. The area of immiscible HEAs is yet to be thoroughly researched, and the feasibility of this particular system in laser cladding on aluminum alloy surfaces remains to be validated. Further confirmation is also needed regarding incorporating ceramic reinforcing phases into HEAs. Furthermore, from an industrial perspective, implementing high-entropy alloys, which often come with high melting points and costs, still requires more in-depth exploration.

**Table 7.** Key findings on HEA coatings.

Authors	Coating Material	Key Findings
Shon et al. [108]	AlCrFeCoNi HEA	Reduced defects like coating porosity and cracking through high-energy density multi-layer cladding.
Siddiqui et al. [109]	Mixed powders of Cu, Fe, Ni, Ti	Hardness reached 18 times that of substrate.
Ye et al. [110]	$Al_xFeCoNiCuCr$ HEA	As Al content increased, hardness increased from 390 to 687 HV <sub>0.2</sub> .
Ma et al. [111]	Al, Cu, Ti in FeCoNiCr HEA	Synergistic effect led to high hardness and wear resistance.
Li et al. [114]	$Al_{0.8}FeCoNiCrCu_{0.5}Si_x$ HEAs	Increasing Si content shifted structure; highest hardness achieved with $Al_{0.8}FeCoNiCrCu_{0.5}Si_{0.4}$ , with wear resistance being five to seven times the substrate's.

## 5. Discussion and Suggestions

In terms of metal-based coatings, aluminum-based coatings have demonstrated their reparative prowess in laser cladding on aluminum alloy surfaces. For instance, researchers such as Meinert [57] applied the 4000 series of aluminum alloys to the 6061 and 7075 aluminum alloys. Given the ability of laser cladding to target damaged areas with precision and carry out repairs swiftly, this method circumvents the excessive heating and enlarged heat-affected zones that traditional repair methods might induce. The thermal property compatibility between aluminum-based coatings and the base material renders the laser cladding of aluminum alloy surfaces with aluminum-based coatings an efficient and cost-effective strategy. Research by scholars like Corbin [59] indicates that heat treatments can enhance coating hardness. However, this process might also escalate residual stresses within the coating, amplifying the risks of cracks and other potential defects. Since both the coating and the base material are aluminum-centric, enhancements in mechanical properties compared to the original material are relatively limited.

Fe-based coatings have notably augmented the mechanical properties of the substrate. The FeCrMoVC coating studied by Jeyaprakash et al. [63], and the Fe alloy with Wt.%Al explored by Tomida et al. [63], showcased remarkable hardness enhancement. Specifically, in the study by Tomida et al. [63], the alloy achieved a significant boost in hardness values, ranging from 600–1000 HV, by introducing 10–40 wt.% Al content. However, a common issue with Fe-based coatings is the formation of cracks. Research by Ye et al. [64] pinpointed that the cracks appearing at the bond interface between the coating and the base material are attributed to Fe-Al intermetallic compounds. These cracks are associated with the internal stresses within these intermetallic compounds and their mismatch with the substrate. The works of Mei et al. [66] and Carroll et al. [67] further substantiated this viewpoint; the presence of multiple brittle intermetallic compounds in the coating leads to its susceptibility to cracking. A solution to the cracking issue might be controlling the composition of these brittle intermetallic compounds prone to inducing cracks. Moreover, adjusting the coating fabrication process might also be method aiming to minimize the formation of intermetallic compounds or alter their morphology and distribution in the coating, thereby optimizing its performance.

Nickel-based alloy coatings are the most widely studied in the realm of metal-based coatings. The TiB<sub>2</sub>-reinforced nickel-based composite researched by He et al. [69], and the NiCrBSi alloy explored by Liang et al. [70], exhibited significant hardness enhancements. The coating developed by He et al. [69] achieved a hardness that was 6.7 times that of the substrate. At the same time, studies by Tan et al. [73], as well as Wang et al. [71], confirmed that, compared to the substrate, nickel-based coatings boast superior wear resistance. Testing wear resistance on aluminum alloy surfaces suggests that nickel-based coatings can be multi-layered on aluminum alloy surfaces, with the bond strength between the coating and substrate exceeding that of Fe-based alloys. However, due to the pronounced physical and chemical differences between the coatings and the substrate, defects such as cracks and porosities can easily form in the coatings. The incorporation of rare-earth elements has been shown to alleviate these issues. However, many rare earth oxides have melting points exceeding the boiling point of aluminum alloys. This implies that during coating preparation, a balance must be struck between ensuring complete powder melting and avoiding excessive dilution or evaporation of the substrate. This necessitates precise control of the laser's thermal input.

Incorporating ceramics into metal bases can notably enhance the substrate's hardness and wear resistance. For instance, in the study by Sun et al. [74], the SiC/Al-12Si composite led to a doubling of the coating layer's hardness, reaching approximately 260 HV<sub>0.2</sub>. Similarly, the Al-Si-based composite containing SiC researched by Yang et al. [77] also showcased the augmented wear resistance of the coating. The extremely high melting points of ceramics pose challenges for their application. In preparing ceramic-inclusive coatings, there is a need to control the thermal input of the laser precisely.

Research on laser cladding for aluminum alloy surfaces is primarily focused on two emerging types of coatings: amorphous alloys and high-entropy alloys. Amorphous alloys, characterized by long-range disorder and short-range order similar to glass, are formed by suppressing nucleation during the solidification of molten materials. Due to their absence of crystallographic defects such as vacancies, dislocations, and stacking faults, these materials theoretically possess superior properties such as high hardness, wear resistance, and corrosion resistance. Studies by Sohrabi et al. [87] and Wang et al. [88] highlight the potential of amorphous coatings when laser clad onto aluminum alloy surfaces, significantly enhancing the substrate's wear resistance. Future research should focus on reducing or eliminating segregation in the coating during the laser cladding process to achieve a uniform and defect-free amorphous layer.

Laser-clad HEA coatings have been proven to enhance aluminum alloy surfaces' hardness, wear resistance, and corrosion resistance. Researchers like Siddiqui [109], Ye [110], and Ma et al. [111], through their respective studies, have revealed the advantages of HEAs. By introducing elements like Al and Si, we can enhance the coating's performance. However, HEA research is still in its early stages and lacks a solid theoretical basis. The high-temperature attributes of laser-clad HEAs are primarily limited to basic properties such as hardness and resistance to oxidation. Comprehensive studies on their high-temperature behaviors, like creep and thermal fatigue, are absent. The rapid cooling in the laser cladding of HEAs occurs under non-equilibrium conditions, and the underlying mechanisms are not well understood. The industrial applications of laser-clad HEAs are limited, with many process parameters being experimentally optimized. Future research can aim to develop a design model for laser-clad HEAs, explore the underlying scientific theories of component design, and expand on current alloy theories to understand the component–structure–performance interplay better. Additionally, in-depth studies into these HEAs' solidification dynamics and complex structures under non-equilibrium conditions are vital.

Consolidating the research findings above, Table 8 provides an integrated overview of various coating types, their recommended application environments, expected performance, and pertinent precautions.

**Table 8.** Comparative analysis of coating types, their application recommendations, expected outcomes, and implementation precautions.

Coating Type	Recommended Application Environment/Conditions	Expected Performance	Precautions
Aluminum-based coating	Component repair sectors; areas with low surface performance demands	Hardness and corrosion resistance are similar to the base material	Heat treatment can enhance mechanical properties and ensure process control to prevent coating from cracking.
Iron-based coating	Low-cost coating needs; high surface hardness domains	High surface hardness	Limited improvement in corrosion resistance; the coating has high crack sensitivity.
Nickel-based coating	Cost-insensitive areas; high hardness and wear resistance domains	High surface hardness, wear resistance, and moderate corrosion resistance	Add rare earth elements to reduce cracks; monitor laser heat closely.
Ceramic-based Coating	High hardness and wear resistance domains	High surface hardness and wear resistance	Strong crack sensitivity; complex reaction products. Process control is essential.
Amorphous alloy Coating	Wear-resistant domains; cost-insensitive areas	Decent hardness and wear resistance	Emerging coating with limited research; the practical application needs verification.
High-Entropy alloy Coating	Cost-insensitive areas; high hardness, wear, and corrosion resistance domains	High surface hardness, wear and corrosion resistance	Coating is expensive. Utilize the “cocktail effect” of high-entropy alloys; regulate Al, Si, Ti, and Cr components and composition for performance tuning.

## 6. Conclusions

The failure and scrapping of mechanical equipment under harsh conditions cause substantial economic losses to industrial production. Laser cladding technology provides a rapid and environmentally friendly approach to the surface strengthening and remanufacturing of workpieces. It effectively improves the surface properties of aluminum alloys or serves as a surface repair technology for these alloys. At present, the cladding materials for aluminum alloy laser cladding research cover metal-based alloys, ceramic-reinforced composite materials, and some emerging materials, focusing on enhancing the surface hardness, wear resistance, or corrosion resistance of the aluminum alloy based on the different characteristics of the materials.

Although significant achievements and developments have been made in research on laser cladding coatings for aluminum alloy surfaces domestically and abroad in recent years, many key issues are still worthy of further in-depth study and improvement. Due to the inherent difficulties in aluminum alloy laser cladding, such as high laser reflectivity, the ease of forming a high-melting-point oxide film on the aluminum alloy surface during cladding, the high dilution rate of the cladding layer, deviations in the coating composition from the designed nominal composition, and the occurrence of cracks, pores, and other defects, the alloy elements undergo oxidation and burning, leaving aluminum alloy laser cladding primarily in the experimental stage, unable to be applied on a large scale in actual industrial production.

To address the problems in aluminum alloy laser cladding, current solutions mainly focus on the following areas:

(1) Composition design and control of the cladding layer material. Based on traditional composition design, and considering the process characteristics of laser cladding technology, cladding powder systems are designed for aluminum alloy laser cladding conditions. This includes developing emerging cladding layers, adding absorbers to enhance laser

absorption capacity, adding rare earth elements to improve the flowability of the molten pool, the in situ generation of ceramic materials, and the research and development of gradient coatings.

(2) Regulation of laser process parameters and the research and development of other auxiliary technologies. Reasonable control of laser power, scanning speed, powder feed rate, and other laser process parameters is required to establish an appropriate aluminum alloy laser cladding process parameter window. Simultaneously, the introduction of auxiliary technologies such as electric fields, magnetic fields, ultrasonic vibrations, and the combination of laser cladding with laser shock, micro-forging, etc., can effectively improve the distribution of residual stress, suppress the problems of cracks and pores in the cladding layer, and enhance the fatigue resistance and other comprehensive properties of the samples.

(3) Pre-treatment and heat treatment of the aluminum alloy surface. The use of physical or chemical methods to remove the oxide film on the aluminum alloy surface before cladding, preheating of the substrate, and the possible remelting or annealing of the coating after cladding, or other methods, can reduce the temperature difference between the cladding layer material and the aluminum alloy substrate during the laser cladding process, thereby reducing thermal stress and achieving the aim of lowering the amount of cracking of the cladding layer.

To address the current challenges in this area, future endeavors could be channeled into the following areas:

(1) The design of novel cladding material composition and gradient structures: Current efforts have explored the potential of amorphous alloys and HEAs as coatings. However, due to the large linear expansion coefficient, high thermal conductivity, and relatively low elastic modulus of aluminum alloys, there is significant difficulty in matching the thermophysical properties of the surface reinforcement layer material to the alloy. To circumvent the pronounced thermophysical disparities between the coating and the substrate, the design of cladding layer materials can be approached by achieving a gradient change in the powder layer composition and in situ generation on the surface. Incorporating emerging materials, like gradient amorphous coatings and gradient HEA coatings, may pave the way for coatings that combine high toughness at the interface with the substrate and hardness at the surface, fulfilling the promise of innovative coatings.

(2) The optimization and control of the interface between reinforcement particles and the matrix: The rapid cooling and solidification process inherent to laser cladding results in structural and performance variations at the interface between the particles and the matrix, as compared to those obtained through comprehensive reaction processes such as sintering and casting. Given that the interfacial performance significantly influences the composite coating's overall attributes, harnessing techniques like process optimization and material compatibility assessments is imperative to achieve superior interface properties.

(3) The development of advanced laser cladding systems: This entails the creation of high-powered, short-wavelength lasers to augment the energy density and cladding efficiency of aluminum alloy laser cladding. Additionally, there is a need to set up a comprehensive database dedicated to aluminum alloy laser cladding. Such a database would aim to establish benchmarks and repositories for accurately evaluating cladding materials, processing parameters, and structural attributes, aligning with the emerging trends of digitalization and informatization.

**Author Contributions:** Conceptualization, P.Z.; methodology, Z.S.; validation, Y.L.; formal analysis, Y.L.; investigation, Y.L.; resources, Z.S.; data curation, X.W.; writing—original draft preparation, Y.L.; writing—review and editing, Y.L.; visualization, Y.L. and M.Z.; supervision, Z.C.; project administration, X.W.; and funding acquisition, M.Z. and J.L. All authors have read and agreed to the published version of the manuscript.

**Funding:** This study was supported by the Natural Science Research Project of Anhui Provincial Department of Education (Grant Nos. KJ2021A0947), Anhui Provincial Major Science and Technology Project (202003c08020002), the University-level natural science research project of West Anhui University (Grant Nos. WXZR202116, WGKQ2021068), the High-level Talents Research Project of West Anhui University (Grant No. WGKQ2021068, WGKQ 201802004). The Key Science and Technology Program of Anhui Province of China (2021001), the Key generic technology research and development project of Hefei City (2021GJ053), the Natural Science Foundation of Anhui Province (2108085ME142), the National Natural Science Foundation of China [52001304], the Science and Technology Program of Inner Mongolia Autonomous Region (2022YFDZ0004).

**Data Availability Statement:** The data that support the findings in this study are available from the author Y.L. upon reasonable request.

**Conflicts of Interest:** The authors declare no conflict of interest.

## References

1. Dixit, A.; Kumar, K. Optimization of Mechanical Properties of Silica Gel Reinforced Aluminium MMC by using Taguchi Method. *Mater. Today-Proc.* **2015**, *2*, 2359–2366. [\[CrossRef\]](#)
2. Doshi, S.J.; Gohil, A.V.; Mehta, N.; Vaghasiya, S. Challenges in Fusion Welding of Al alloy for Body in White. *Mater. Today-Proc.* **2018**, *5*, 6370–6375. [\[CrossRef\]](#)
3. Feng, M.N.; Xie, Y.; Zhao, C.F.; Luo, Z. Microstructure and mechanical performance of ultrasonic spot welded open-cell Cu foam/Al joint. *J. Manuf. Process.* **2018**, *33*, 86–95. [\[CrossRef\]](#)
4. Sun, X.; Jie, J.; Peng, B.; Dong, G.; Liu, J.; Liu, S.; Li, T. Numerical Study and Experimental Verification on Solidification Characteristics in Commercial Purity Aluminum under Mechanical Vibration. *J. Mater. Eng. Perform.* **2023**, 1–8. [\[CrossRef\]](#)
5. Wang, B.; An, X.; Xue, P.; Liu, F.; Ni, D.; Xiao, B.; Liu, Y.; Ma, Z. Grain size effects on high cycle fatigue behaviors of pure aluminum. *Int. J. Fatigue* **2023**, *170*, 107556. [\[CrossRef\]](#)
6. Yamagishi, H. Cu/Al Dissimilar Cold Spot Forge Welding: Effects of Bonding Temperature and Reduction Ratio on Joint Strength and Reaction Layer Growth. *Met. Mater. Trans. A Phys. Metall. Mater. Sci.* **2023**, *54*, 3519–3536. [\[CrossRef\]](#)
7. Li, J.; Wang, G.; Zhang, M.; Li, J.; Fang, X.; Ma, X. Strengthening mechanisms of a heterostructured pure aluminum with extraordinary mechanical properties. *Mater. Charact.* **2023**, *202*, 113049. [\[CrossRef\]](#)
8. Singh, B.; Kumar, I.; Saxena, K.K.; Mohammed, K.A.; Khan, M.I.; Ben Moussa, S.; Abdullaev, S.S. A future prospects and current scenario of aluminium metal matrix composites characteristics. *Alex. Eng. J.* **2023**, *76*, 1–17. [\[CrossRef\]](#)
9. Liu, M.; Xu, Z.; Yang, F. Characterization of cyclic dynamic and creep responses of pure aluminum by instrumented indentation. *Sci. Sin. Phys. Mech. Astron.* **2023**, *53*, 214605. [\[CrossRef\]](#)
10. Scharifi, E.; Yardley, V.A.; Weidig, U.; Szegda, D.; Lin, J.; Steinhoff, K. Hot Sheet Metal Forming Strategies for High-Strength Aluminum Alloys: A Review—Fundamentals and Applications. *Adv. Eng. Mater.* **2023**, *25*, 2300141. [\[CrossRef\]](#)
11. Chinh, N.Q.; Olasz, D.; Ahmed, A.Q.; Bobruk, E.V.; Valiev, R.Z. Review on Grain Size- and Grain Boundary Phenomenon in Unusual Mechanical Behavior of Ultra fine-Grained Al Alloys. *Mater. Trans.* **2023**, *64*, 1844–1855. [\[CrossRef\]](#)
12. Kumar, P.K.D.; Gnanaraj, S.D. Aluminium-Silicon based Metal Matrix Composites for brake rotor applications: A review. *Eng. Res. Express* **2023**, *5*, 022002. [\[CrossRef\]](#)
13. Eskandarzade, M.; Masalehdan, T.; Tutunchi, A.; Osouli-Bostanabad, K.; Hildyard, R.; Bewsher, S.R.; Mohammadpour, M. Study of Tribological Properties of Bulk Nanostructured Aluminum and Copper Samples Applicable in Automotive Bearing Application. *J. Mater. Eng. Perform.* **2023**, *32*, 8807–8817. [\[CrossRef\]](#)
14. Yuan, L.; Zeng, X.; Zhao, X.; Xie, Y.; Gandra, J.; Guan, D. Microstructure evolution and tensile behaviour of fine-grained 6082 Al wire with high ultimate strength and high work hardening by friction stir extrusion of bulk Al sheet. *Mater. Sci. Eng. A* **2023**, *864*, 144589. [\[CrossRef\]](#)
15. Ashebir, D.A.; Mengesha, G.A.; Sinha, D.K.; Bereda, Y.B. Multi-response optimization of process and reinforcement parameters of hybrid reinforced Al matrix composites using Taguchi-Grey relational analysis. *Eng. Res. Express* **2022**, *4*, 045038. [\[CrossRef\]](#)
16. Shahri, S.E.E.; Gholami, M.; Rakhshkhorshid, M. Numerical-experimental study of die geometry in the constrained groove pressing of 6061 aluminum sheets. *Proc. Inst. Mech. Eng. Part B J. Eng. Manuf.* **2022**, *237*, 1836–1846. [\[CrossRef\]](#)
17. Pungaiah, S.S.; Sahu, K.K.; Yuvaraja, R.; Prabhu, G.J.; Sudharsan, R.R.; Thamizhvalavan, P.; Ramaswamy, K. Investigation on Mechanical Behaviour of LM6 Aluminum Alloy Hybrid Composites Processed Using Stir Casting Process. *Adv. Mater. Sci. Eng.* **2022**, *2022*, 7539546.
18. Mahmoud, E.R.I.; Khan, S.Z.; Aljabri, A.; Almohamadi, H.; Elkotb, M.A.; Gepreel, M.A.; Ebied, S. Free Intermetallic Cladding Interface between Aluminum and Steel through Friction Stir Processing. *Crystals* **2022**, *12*, 1413. [\[CrossRef\]](#)
19. Niu, G.; Wang, J.; Ye, J.; Mao, J. Enhancing Fe content tolerance in A356 alloys for achieving low carbon footprint aluminum structure castings. *J. Mater. Sci. Technol.* **2023**, *161*, 180–191. [\[CrossRef\]](#)
20. Wang, J.; Li, F. Effect of Sm + Er and Heat Treatment on As-Cast Microstructure and Mechanical Properties of 7055 Aluminum Alloy. *Materials* **2023**, *16*, 4846. [\[CrossRef\]](#)

21. Thanabumrungkul, S.; Jumpol, W.; Meemongkol, N.; Wannasin, J. Investment casting of semi-solid 6063 aluminum alloy using the GISS process. *Mater. Res. Express* **2023**, *10*, 076501. [[CrossRef](#)]
22. Wang, L.X.; Yin, K.; Deng, Q.W.; Huang, Q.Q.; He, J.; Duan, J.A. Wetting Ridge-Guided Directional Water Self-Transport. *Adv. Sci.* **2022**, *9*, 2204891. [[CrossRef](#)]
23. Yang, D.; Tang, S.; Wu, Z.; Qin, K.; Zhang, H.; Cui, J.; Nagaumi, H. Research Status and Development Trend of Alloying and Process Technology of High-zinc Aluminum Alloy. *Mater. Rev.* **2023**, *37*, 134–139.
24. Li, Q.; Sun, J.; Ren, X.; Hu, M. Effects of High Temperature RRA on Microstructure and Properties of 7075 Aluminum Alloy. *Hot Work. Technol.* **2018**, *47*, 129–132, 137.
25. Mironov, A.E.; Gershman, I.S.; Gershman, E.I.; Zheleznov, M.M. Relationship between the Tribological Properties of Experimental Aluminum Alloys and Their Chemical Composition. *J. Frict. Wear* **2017**, *38*, 87–91. [[CrossRef](#)]
26. Li, Y.Z.; Shi, Y.; Olugbade, E. Microstructure, mechanical, and corrosion resistance properties of  $Al_{0.8}CrFeCoNiCu_x$  high-entropy alloy coatings on aluminum by laser cladding. *Mater. Res. Express* **2020**, *7*, 026504. [[CrossRef](#)]
27. Li, Y.Z.; Shi, Y. Microstructure and wear resistance of the laser-cladded  $Al_{0.8}CrFeCoNiCu_{0.5}B_x$  high-entropy alloy coating on aluminum. *Mater. Res. Express* **2020**, *7*, 026517. [[CrossRef](#)]
28. Li, Y.; Shi, Y. Microhardness, wear resistance, and corrosion resistance of  $Al_xCrFeCoNiCu$  high-entropy alloy coatings on aluminum by laser cladding. *Opt. Laser Technol.* **2021**, *134*, 106632. [[CrossRef](#)]
29. Zhang, Y.; Gao, M.; Chen, T.; Pan, L.; Wu, M. Study on the Corrosion Resistance of Thermal Spraying Zinc Aluminum Coating with High Aluminum Content. *Mater. Prot.* **2021**, *54*, 28–33.
30. Riah, B.; Ayad, A.; Camus, J.; Rammal, M.; Boukari, F.; Chekour, L.; Djouadi, M.; Rouag, N. Textured hexagonal and cubic phases of AlN films deposited on Si (100) by DC magnetron sputtering and high power impulse magnetron sputtering. *Thin Solid Films* **2018**, *655*, 34–40. [[CrossRef](#)]
31. Zhang, J.; Song, B.; Wei, Q.; Bourell, D.; Shi, Y. A review of selective laser melting of aluminum alloys: Processing, microstructure, property and developing trends. *J. Mater. Sci. Technol.* **2019**, *35*, 270–284. [[CrossRef](#)]
32. Wang, C.; Wu, G.; Zhang, Q.; Zhang, Y.; Xiu, Z.; Chen, G. A Review for Corrosion Resistance and Protection Methods for Aluminum Matrix Composites. *J. Chin. Soc. Corros. Prot.* **2008**, *28*, 59–64.
33. Chen, B.; Li, Y.; Nie, J.; Wei, C.; Dang, L.; Ma, Q. Microstructure and mechanical properties of NiCoCrAlY laser cladding coating after high-current pulsed electron beam irradiation. *Philos. Mag. Lett.* **2023**, *103*, 2191223. [[CrossRef](#)]
34. Jing, Z.; Xu, P.; Liu, Q.; Yu, C. Residual stress release during laser cladding process: A review. *J. Laser Appl.* **2023**, *35*, 031201. [[CrossRef](#)]
35. Jiang, L.; Cui, X.; Jin, G.; Tian, Z.; Wen, X.; Tian, H.; Liu, E. Design and characterization of a novel  $Cu_{2.3}Al_{1.3}Ni_{1.7}SnCr_{0.3}$  multi-principal element alloy coating on magnesium alloy by laser cladding. *J. Mater. Sci. Technol.* **2023**, *152*, 220–236. [[CrossRef](#)]
36. Arif, Z.U.; Khalid, M.Y.; Rehman, E.U.; Ullah, S.; Atif, M.; Tariq, A. A review on laser cladding of high-entropy alloys, their recent trends and potential applications. *J. Manuf. Process.* **2021**, *68*, 225–273. [[CrossRef](#)]
37. Liu, Y.; Ding, Y.; Yang, L.; Sun, R.; Zhang, T.; Yang, X. Research and progress of laser cladding on engineering alloys: A review. *J. Manuf. Process.* **2021**, *66*, 341–363. [[CrossRef](#)]
38. Siddiqui, A.A.; Dubey, A.K. Recent trends in laser cladding and surface alloying. *Opt. Laser Technol.* **2021**, *134*, 106619. [[CrossRef](#)]
39. Liu, M.; Duan, C.; Li, G.; Cai, Y.; Li, L.; Wang, F. Multi-indicator evaluation and material selection of hybrid additive-subtractive manufacturing to repair automobile panel dies and molds. *Int. J. Adv. Manuf. Technol.* **2023**, *127*, 1675–1690. [[CrossRef](#)]
40. Izumi, T.; Arai, M. Numerical simulation of the 3D propeller repair process by laser cladding of SUS316L on SUS304. *J. Manuf. Process.* **2023**, *98*, 234–253. [[CrossRef](#)]
41. Gao, Y.; Lu, P.; Bai, S.; Qin, B.; Zhang, D. Influence of Laser Power on Microstructure and Properties of Al-Si+ $Y_2O_3$  Coating. *Coatings* **2023**, *13*, 1289. [[CrossRef](#)]
42. Huang, Q.; Yin, K.; Wang, L.; Deng, Q.; Arnusch, C.J. Femtosecond laser-scribed superhydrophilic/superhydrophobic self-splitting patterns for one droplet multi-detection. *Nanoscale* **2023**, *15*, 11247–11254. [[CrossRef](#)] [[PubMed](#)]
43. Zuo, T.C.; Chen, K. Laser manufacturing technology and its application on the surface engineering. In *Contributions of Surface Engineering to Modern Manufacturing and Remanufacturing*; Southwest Jiaotong University Press: Chengdu, China, 2002.
44. Ozdemir, M.; Sadikoglu, H. A new and emerging technology: Laser-induced surface modification of polymers. *Trends Food Sci. Technol.* **1998**, *9*, 159–167. [[CrossRef](#)]
45. Folkes, J. Surface modification and coating with lasers. In *Surface Coatings for Advanced Materials*; Agarwala, R.P., Ed.; Universities in Chicago: Chicago, America, 1997; Volume 246, pp. 261–277.
46. Chen, J.F.; Li, X.C.; Wang, J.T.; Lei, W.N. Effect of  $CO_2$  Laser Surface Melting on the Microstructure of AZ91D Magnesium Alloy. *Key Eng. Mater.* **2011**, *464*, 461–464. [[CrossRef](#)]
47. Han, S.W.; Joo, B.D.; Moon, Y.H. Selective surface hardening by laser melting of alloying powder. *Mater. Res. Innov.* **2014**, *18*, S2-902. [[CrossRef](#)]
48. Lee, J.H.; Jang, J.H.; Joo, B.D.; Son, Y.M.; Moon, Y.H. Laser surface hardening of AISI H13 tool steel. *Trans. Nonferrous Met. Soc. China* **2009**, *19*, 917–920. [[CrossRef](#)]
49. Huang, X.B. Research and application of laser shock processing. In Proceedings of the ICOSM 2020: Optoelectronic Science and Materials, Hefei, China, 25–27 September 2020; Volume 11606, pp. 119–123.

50. Zhou, M.; Zhang, Y.; Cai, L. Laser shock forming on coated metal sheets characterized by ultrahigh-strain-rate plastic deformation. *J. Appl. Phys.* **2002**, *91*, 5501–5503. [[CrossRef](#)]
51. Lai, Z.L.; Wang, C.; He, W.F.; Zhou, L.C.; Bin An, Z. Application of High-Energy Laser in Strain-Hardening of Material. *Appl. Mech. Mater.* **2013**, *321–324*, 141–145. [[CrossRef](#)]
52. Zhou, Y.; Zhang, K.; Liang, Y.; Cheng, J.; Dai, Y. Selective Laser Melted Magnesium Alloys: Fabrication, Microstructure and Property. *Materials* **2022**, *15*, 7049. [[CrossRef](#)]
53. Knyzeva, A.G.; Sharkeev, Y.P. Two-Dimensional Model of Laser Alloying of Binary Alloy Powder with Interval of Melting Temperature. In Proceedings of the XXV Conference on High-Energy Processes in Condensed Matter (HEPCM 2017), Novosibirsk, Russia, 5–9 June 2017.
54. John, M.; Kuruveri, U.B.; Menezes, P.L. Laser Cladding-Based Surface Modification of Carbon Steel and High-Alloy Steel for Extreme Condition Applications. *Coatings* **2022**, *12*, 1444. [[CrossRef](#)]
55. Cheng, J.; Xing, Y.; Dong, E.; Zhao, L.; Liu, H.; Chang, T.; Chen, M.; Wang, J.; Lu, J.; Wan, J. An Overview of Laser Metal Deposition for Cladding: Defect Formation Mechanisms, Defect Suppression Methods and Performance Improvements of Laser-Cladded Layers. *Materials* **2022**, *15*, 5522. [[CrossRef](#)] [[PubMed](#)]
56. Weng, F.; Chen, C.; Yu, H. Research status of laser cladding on titanium and its alloys: A review. *Mater. Des.* **2014**, *58*, 412–425. [[CrossRef](#)]
57. Meinert, K.C.; Bergan, P. Refurbishment of aluminum alloys by laser cladding. In Proceedings of the ICALEO'99: Proceedings of the Laser Materials Processing Conference, San Diego, CA USA, 15–18 November 1999.
58. Cottam, R.; Luzin, V.; Liu, Q.; Wong, Y.C.; Wang, J.; Brandt, M. Investigation into Heat Treatment and Residual Stress in Laser Clad AA7075 Powder on AA7075 Substrate. *Met. Microstruct. Anal.* **2013**, *2*, 205–212. [[CrossRef](#)]
59. Grohol, C.M.; Shin, Y.C.; Frank, A. Laser cladding of aluminum alloy 6061 via off-axis powder injection. *Surf. Coat. Technol.* **2021**, *415*, 127099. [[CrossRef](#)]
60. Yang, Z.; Wang, A.; Weng, Z.; Xiong, D.; Ye, B.; Qi, X. Porosity elimination and heat treatment of diode laser-clad homogeneous coating on cast aluminum-copper alloy. *Surf. Coatings Technol.* **2017**, *321*, 26–35. [[CrossRef](#)]
61. Song, M.; Wu, L.; Liu, J.; Hu, Y. Effects of laser cladding on crack resistance improvement for aluminum alloy used in aircraft skin. *Opt. Laser Technol.* **2021**, *133*, 106531. [[CrossRef](#)]
62. Dubourg, L.; Pelletier, H.; Vaissiere, D.; Hlawka, F.; Cornet, A. Mechanical characterisation of laser surface alloyed aluminium–copper systems. *Wear* **2002**, *253*, 1077–1085. [[CrossRef](#)]
63. Jeyaprakash, N.; Yang, C.-H.; Sivasankaran, S. Formation of FeCrMoVC Layers on AA6061 by Laser Cladding Process: Microstructure and Wear Characteristics. *Trans. Indian Inst. Met.* **2020**, *73*, 1611–1617. [[CrossRef](#)]
64. Sathiyamoorthi, P.; Kim, H.S. High-entropy alloys with heterogeneous microstructure: Processing and mechanical properties. *Prog. Mater. Sci.* **2022**, *123*, 100709. [[CrossRef](#)]
65. Tomida, S.; Nakata, K. Fe–Al composite layers on aluminum alloy formed by laser surface alloying with iron powder. *Surf. Coatings Technol.* **2003**, *174–175*, 559–563. [[CrossRef](#)]
66. Mei, Z.; Wang, W.; Wang, A. Transmission electron microscopy characterization of laser-clad iron-based alloy on Al–Si alloy. *Mater. Charact.* **2006**, *56*, 185–191. [[CrossRef](#)]
67. Carroll, J.W.; Liu, Y.; Mazumder, J.; Perry, T.A. Laser surface alloying of aluminum 319 alloy with iron. In Proceedings of the 20th International Congress on Applications of Lasers and Electro-Optics (ICALEO 2001), Jacksonville, FL, USA, 14–18 October 2001.
68. Wu, X.Q.; Yan, H.; Xin, Y.; Yu, B.B.; Hu, Z.; Sun, Y.H. Microstructure and Wear Properties of Ni-based Composite Coatings on Aluminum Alloy Prepared by Laser Cladding. *Rare Met. Mater. Eng.* **2020**, *49*, 2574–2582.
69. He, L.; Tan, Y.F.; Wang, X.L.; Jing, Q.F.; Hong, X. Tribological properties of laser cladding TiB<sub>2</sub> particles reinforced Ni-base alloy composite coatings on aluminum alloy. *Rare Met.* **2015**, *34*, 789–796. [[CrossRef](#)]
70. Liang, G.; Su, J. The microstructure and tribological characteristics of laser-clad Ni–Cr–Al coatings on aluminium alloy. *Mater. Sci. Eng. A Struct. Mater. Prop. Microstruct. Process.* **2000**, *290*, 207–212. [[CrossRef](#)]
71. Wang, C.; Gao, Y.; Zeng, Z.; Fu, Y. Effect of rare-earth on friction and wear properties of laser cladding Ni-based coatings on 6063Al. *J. Alloys Compd.* **2017**, *727*, 278–285. [[CrossRef](#)]
72. Zhang, P.F.; Li, Y.X. Effects of CeO<sub>2</sub>, Si and Co on the microstructure and properties of Ni–Cu composite coating on 6061 aluminium alloy by laser cladding. *Philos. Mag. Lett.* **2021**, *101*, 303–311. [[CrossRef](#)]
73. Tan, Y.F.; He, L.; Wang, X.L.; Tan, H.; Zhou, C.H. Tribological properties of laser surface cladding Ni-base alloy coatings under dry friction and seawater conditions. *Int. J. Surf. Sci. Eng.* **2016**, *10*, 147–161. [[CrossRef](#)]
74. Sun, R.; Lei, Y. Microstructure and hardness of laser clad SiCp–Al composite coatings on Al alloys. *Mater. Lett.* **2008**, *62*, 3272–3275. [[CrossRef](#)]
75. Anandkumar, R.; Almeida, A.; Colaco, R.; Vilar, R.; Ocelik, V.; De Hosson, J.T.M. Microstructure and wear studies of laser clad Al–Si/SiC(p) composite coatings. *Surf. Coat. Technol.* **2007**, *201*, 9497–9505. [[CrossRef](#)]
76. Anandkumar, R.; Almeida, A.; Vilar, R. Microstructure and sliding wear resistance of an Al–12 wt.% Si/TiC laser clad coating. *Wear* **2012**, *282*, 31–39. [[CrossRef](#)]
77. Liu, Y.; Li, G.D.; Jiang, W.T. Effects of Cu-Coated SiC Content on Microstructure and Properties of Laser Cladding SiCp/Al–Si Composite Coatings. *Materials* **2019**, *12*, 1537. [[CrossRef](#)]

78. Li, Y.; Zhang, P.; Bai, P.; Wu, L.; Liu, B.; Zhao, Z. Microstructure and properties of Ti/TiBCN coating on 7075 aluminum alloy by laser cladding. *Surf. Coatings Technol.* **2018**, *334*, 142–149. [[CrossRef](#)]
79. Riquelme, A.; Escalera-Rodríguez, M.D.; Rodrigo, P.; Otero, E.; Rams, J. Effect of alloy elements added on microstructure and hardening of Al/SiC laser clad coatings. *J. Alloys Compd.* **2017**, *727*, 671–682. [[CrossRef](#)]
80. Al-Hamdani, K.S.; Murray, J.W.; Hussain, T.; Clare, A.T. Controlling ceramic-reinforcement distribution in laser cladding of MMCs. *Surf. Coatings Technol.* **2019**, *381*, 125128. [[CrossRef](#)]
81. Ayerdi, J.J.; Aginagalde, A.; Llavori, I.; Bonse, J.; Zabala, A.J.W. Ball-on-flat linear reciprocating tests: Critical assessment of wear volume determination methods and suggested improvements for ASTM D7755 standard. *Wear* **2021**, *470–471*, 203620. [[CrossRef](#)]
82. Yu, J.; Qiao, C.; Zhang, S.; Liu, Z.; Wróblewski, P. Tribological properties of laser-cladded Fe-based amorphous composite coatings under dry and lubricated sliding. *Opt. Laser Technol.* **2023**, *166*, 109583. [[CrossRef](#)]
83. Zhang, Z.; Yuan, J.; Jing, Z.; Cheng, Y.; Liang, X. Research Progress and Development Trend of Amorphous and Nanocrystalline Composite Coatings: A Review. *JOM* **2022**, *74*, 4597–4611. [[CrossRef](#)]
84. Zhang, Y.H.; Xu, J.F.; Hu, Y.Q.; Ding, S.H.; Xia, R. Cold welding of ultrathin metallic glass nanowires with side-to-side contact using molecular dynamics simulations. *Mater. Today Commun.* **2022**, *32*, 103937. [[CrossRef](#)]
85. Song, S.; Laurell, F.; Meehan, B.; Hawkins, T.W.; Ballato, J.; Gibson, U.J. Localised structuring of metal-semiconductor cores in silica clad fibres using laser-driven thermal gradients. *Nat. Commun.* **2022**, *13*, 2680. [[CrossRef](#)]
86. Ibrahim, M.Z.; Halilu, A.; Sarhan, A.A.; Kuo, T.; Yusuf, F.; Shaikh, M.; Hamdi, M. In-vitro viability of laser cladded Fe-based metallic glass as a promising bioactive material for improved osseointegration of orthopedic implants. *Med. Eng. Phys.* **2022**, *102*, 103782. [[CrossRef](#)]
87. Sohrabi, N.; Panikar, R.S.; Jhabvala, J.; Buch, A.R.; Mischler, S.; Logé, R.E. Laser coating of a Zr-based metallic glass on an aluminum substrate. *Surf. Coatings Technol.* **2020**, *400*, 126223. [[CrossRef](#)]
88. Wang, Y.; Ostrowska, M.; Cacciamani, G. Thermodynamic modeling of selected ternary systems containing Y and CALPHAD simulation of CoNiCrAlY metallic coatings. *Calphad* **2021**, *72*, 102214. [[CrossRef](#)]
89. Yan, J.; Zhang, P.; Liu, J.; Yu, H.; Hu, Q.; Yang, J.; Zhang, Z. Design and optimization of the composition and mechanical properties for non-equiatom CoCrNi medium-entropy alloys. *J. Mater. Sci. Technol.* **2023**, *139*, 232–244. [[CrossRef](#)]
90. Huang, A.; Fensin, S.J.; Meyers, M.A. Strain-rate effects and dynamic behavior of high entropy alloys. *J. Mater. Res. Technol.* **2023**, *22*, 307–347. [[CrossRef](#)]
91. Laleh, M.; Sadeghi, E.; Revilla, R.I.; Chao, Q.; Haghdadi, N.; Hughes, A.E.; Xu, W.; De Graeve, I.; Qian, M.; Gibson, I.; et al. Heat treatment for metal additive manufacturing. *Prog. Mater. Sci.* **2023**, *133*, 101051. [[CrossRef](#)]
92. Meena, N.; Rao, A.G.; Dommeti, S.G.; Prabhu, N. Effect of Multi-Pass Friction Stir Processing on Microstructure and Mechanical Properties of a Metastable Dual-Phase High Entropy Alloy. *Lubricants* **2023**, *11*, 2. [[CrossRef](#)]
93. Li, Y.; Shi, Y.; Wang, H.; Zhou, B.; Li, D.; Lin, H.; Wang, J. Effect of Y on Microstructure and Properties of Al<sub>0.8</sub>FeCrCoNiCu<sub>0.5</sub> High Entropy Alloy Coating on 5083 Aluminum by Laser Cladding. *Lubricants* **2023**, *11*, 50. [[CrossRef](#)]
94. Reverte, E.; Keller, C.; Calvo-Dahlborg, M.; Alcalá, G.; Campos, M.; Cornide, J. Effect of Y<sub>2</sub>O<sub>3</sub> addition on the microstructure and mechanical properties of an Al<sub>1.8</sub>CoCrCu<sub>0.5</sub>FeNi BCC HEA. *J. Alloys Compd.* **2023**, *960*, 170647. [[CrossRef](#)]
95. Wen, J.; Liu, Y.; Huang, Y.; Zhao, Y. Effects of electromagnetic stirring and subsequent homogenization treatment on the microstructure and mechanical properties of Al<sub>70</sub>Zn<sub>10</sub>Mg<sub>10</sub>Cu<sub>5</sub>Si<sub>5</sub> multi-component alloy. *J. Alloys Compd.* **2023**, *960*, 170725. [[CrossRef](#)]
96. Yang, B.; Fang, J.; Xu, C.; Cao, H.; Zhang, R.; Zhao, B.; Huang, M.; Wang, X.; Lv, H.; Che, R. One-Dimensional Magnetic FeCoNi Alloy Toward Low-Frequency Electromagnetic Wave Absorption. *Nano-Micro Lett.* **2022**, *14*, 170. [[CrossRef](#)]
97. Xiong, W.; Guo, A.X.; Zhan, S.; Liu, C.-T.; Cao, S.C. Refractory high-entropy alloys: A focused review of preparation methods and properties. *J. Mater. Sci. Technol.* **2023**, *142*, 196–215. [[CrossRef](#)]
98. Li, H.; Han, Y.; Feng, H.; Zhou, G.; Jiang, Z.; Cai, M.; Li, Y.; Huang, M. Enhanced strength-ductility synergy via high dislocation density-induced strain hardening in nitrogen interstitial CrMnFeCoNi high-entropy alloy. *J. Mater. Sci. Technol.* **2023**, *141*, 184–192. [[CrossRef](#)]
99. Wang, X.; Zhai, W.; Wang, J.; Wei, B. Strength and ductility enhancement of high-entropy FeCoNi<sub>2</sub>Al<sub>0.9</sub> alloy by ultrasonically refining eutectic structures. *Scr. Mater.* **2023**, *225*, 115154. [[CrossRef](#)]
100. Alamiery, A.A.; Isahak, W.N.R.W.; Takriff, M.S. Inhibition of Mild Steel Corrosion by 4-benzyl-1-(4-oxo-4-phenylbutanoyl)thiosemi carbazide: Gravimetric, Adsorption and Theoretical Studies. *Lubricants* **2021**, *9*, 93. [[CrossRef](#)]
101. Zhang, D.; Du, D.; Liu, G.; Pu, Z.; Xue, S.; Chang, B. Microstructure and Wear Resistance of FeCuNiTiAl High-Entropy Alloy Coating on Ti6Al4V Substrate Fabricated by Laser Metal Deposition. *Lubricants* **2022**, *10*, 263. [[CrossRef](#)]
102. Zhang, X.; Tong, Y.; Hu, Y.; Liang, X.; Chen, Y.; Wang, K.; Zhang, M.; Xu, J. Microstructure and Performance of Fe<sub>50</sub>Mn<sub>30</sub>Cr<sub>10</sub>Ni<sub>10</sub> High-Entropy Alloy Produced by High-Efficiency and Low-Cost Wire Arc Additive Manufacturing. *Lubricants* **2022**, *10*, 344. [[CrossRef](#)]
103. Cantor, B. Multicomponent high-entropy Cantor alloys. *Prog. Mater. Sci.* **2021**, *120*, 100754. [[CrossRef](#)]
104. Jin, C.; Li, X.L.; Kang, J.H.; Li, H.Z.; Wang, H.F. Effect of interstitial oxygen/nitrogen on mechanical and wear properties of TiZrHfNb refractory high-entropy alloy. *J. Alloys Compd.* **2023**, *960*, 170863. [[CrossRef](#)]
105. Liu, Q.; Fu, H.; Wu, W.; Wang, L.; Cheng, J.; Xia, P.; Gan, B.; Xia, M.; Zhao, F. Influence of annealing temperatures on the microstructure and deformation behavior of a CrCoNi based medium-entropy alloy. *J. Alloys Compd.* **2023**, *960*, 170877. [[CrossRef](#)]

106. Xu, T.; Chen, Q.; Ji, L.; Zheng, Z.; Wang, K.; Liu, H. BCC/B2 structure and dislocation strengthening behavior in high Ti content TiAlVCrNb high-entropy alloys. *J. Alloys Compd.* **2023**, *956*, 170179. [[CrossRef](#)]
107. Wang, Y.; Chen, Y.; Xie, J.; Ni, J.; Zhang, T.; Wang, S.; Yin, L. Microstructure and mechanical properties of CrMnFeCoNi high entropy alloy/Al composite with different reinforcement content. *J. Alloys Compd.* **2023**, *960*, 170882. [[CrossRef](#)]
108. Shon, Y.; Joshi, S.S.; Katakam, S.; Rajamure, R.S.; Dahotre, N.B. Laser additive synthesis of high entropy alloy coating on aluminum: Corrosion behavior. *Mater. Lett.* **2015**, *142*, 122–125. [[CrossRef](#)]
109. Siddiqui, A.A.; Dubey, A.K.; Paul, C.P. A study of metallurgy and erosion in laser surface alloying of Al<sub>x</sub>Cu<sub>0.5</sub>FeNiTi high entropy alloy. *Surf. Coatings Technol.* **2019**, *361*, 27–34. [[CrossRef](#)]
110. Ye, X.; Ma, M.; Liu, W.; Li, L.; Zhong, M.; Liu, Y.; Wu, Q. Synthesis and Characterization of High-Entropy Alloy FeCoNiCuCr by Laser Cladding. *Adv. Mater. Sci. Eng.* **2011**, *2011*, 485942. [[CrossRef](#)]
111. Ma, Z.; Xia, C.; Zhong, H.; Yang, T.; Liu, N.; Liang, C.; Li, Q. Microstructure, mechanical property and corrosion resistance of FeCoCrNi-M high-entropy alloy coatings on 6061 aluminum alloy prepared by laser cladding. *Surf. Coat. Technol.* **2023**, *455*, 129217. [[CrossRef](#)]
112. Shi, Y.; Ni, C.; Liu, J.; Huang, G. Microstructure and properties of laser clad high-entropy alloy coating on aluminium. *Mater. Sci. Technol.* **2018**, *34*, 1239–1245. [[CrossRef](#)]
113. Ni, C.; Shi, Y.; Liu, J.; Huang, G. Characterization of Al<sub>0.5</sub>FeCu<sub>0.7</sub>NiCoCr high-entropy alloy coating on aluminum alloy by laser cladding. *Opt. Laser Technol.* **2018**, *105*, 257–263. [[CrossRef](#)]
114. Li, Y.Z.; Shi, Y. Phase assemblage and wear resistance of laser-cladding Al<sub>0.8</sub>FeCoNiCrCu<sub>0.5</sub>Si<sub>x</sub> high-entropy alloys on aluminum. *Mater. Res. Express* **2020**, *7*, 086504. [[CrossRef](#)]

**Disclaimer/Publisher's Note:** The statements, opinions and data contained in all publications are solely those of the individual author(s) and contributor(s) and not of MDPI and/or the editor(s). MDPI and/or the editor(s) disclaim responsibility for any injury to people or property resulting from any ideas, methods, instructions or products referred to in the content.